Ore Geology Reviews 65 (2015) 884–899

Contents lists available at ScienceDirect

Ore Geology Reviews

journal homepage: www.elsevier.com/locate/oregeorev

In-situ LA-ICP-MS trace elemental analyses of magnetite: The Bayan Obo Fe-REE-Nb deposit, North China

Xiao-Wen Huang [a], Mei-Fu Zhou [b], Yu-Zhuo Qiu [c], Liang Qi [a,d,*]

[a] State Key Laboratory of Ore Deposit Geochemistry, Institute of Geochemistry, Chinese Academy of Sciences, Guiyang 550002, China
[b] Department of Earth Sciences, The University of Hong Kong, Hong Kong, Hong Kong, China
[c] Guangzhou Institute of Geochemistry, Chinese Academy of Sciences, Guangzhou 510640, China
[d] State Key Laboratory of Continental Dynamics, Department of Geology, Northwest University, Xi'an 710069, China

ARTICLE INFO

Article history:
Received 11 August 2014
Received in revised form 3 September 2014
Accepted 8 September 2014
Available online 18 September 2014

Keywords:
Trace element
LA-ICP-MS
Magnetite
Hematite
Bayan Obo
North China

ABSTRACT

The Bayan Obo Fe-REE-Nb deposit in northern China is the world's largest light REE deposit, and also contains considerable amounts of iron and niobium metals. Although there are numerous studies on the REE mineralization, the origin of the Fe mineralization is not well known. Laser ablation (LA) ICP-MS is used to obtain trace elements of Fe oxides in order to better understand the process involved in the formation of magnetite and hematite associated with the formation of the giant REE deposit. There are banded, disseminated and massive Fe ores with variable amounts of magnetite and hematite at Bayan Obo. Magnetite and hematite from the same ores show similar REE patterns and have similar Mg, Ti, V, Mn, Co, Ni, Zn, Ga, Sn, and Ba contents, indicating a similar origin. Magnetite grains from the banded ores have Al + Mn and Ti + V contents similar to those of banded iron formations (BIF), whereas those from the disseminated and massive ores have Al + Mn and Ti + V contents similar to those of skarn deposits and other types of magmatic-hydrothermal deposits. Magnetite grains from the banded ores with a major gangue mineral of barite have the highest REE contents and show slight moderate REE enrichment, whereas those from other types of ores show light REE enrichment, indicating two stages of REE mineralization associated with Fe mineralization. The Bayan Obo deposit had multiple sources for Fe and REEs. It is likely that sedimentary carbonates provided original REEs and were metasomatized by REE-rich hydrothermal fluids to form the giant REE deposit.

1. Introduction

The Bayan Obo Fe-REE-Nb deposit in Inner Mongolia of North China is the world's largest light REE deposit, and also contains considerable amounts of iron and niobium metals (Bai et al., 1996; Chao et al., 1997; Kynicky et al., 2012). The deposit was originally discovered as a major magnetite and hematite orebody (Bai, 2012). Numerous studies of REE mineralogy, mineralization age, geochemistry of carbonatite, and ore-forming fluids are available, but the genesis of the deposit has been a matter of debate (Bai et al., 1996; Fan et al., 2014; IGCAS (Institute of Geochemistry, Chinese Academy of Sciences), 1988; Smith and Wu, 2013; Smith et al., 2015; Zhang et al., 2003). Most of the previous studies focused on the origin of REEs, but the origin of Fe mineralization remains controversial. Fe oxides, magnetite and hematite, are widespread in the deposit, and thus the geochemistry of these Fe oxides would provide direct constraints on the source(s) of Fe, and by inference, other ore materials.

Magnetite is common in igneous, metamorphic, and sedimentary rocks and can occur as ore minerals in many types of deposits (Dupuis and Beaudoin, 2011). Magnetite contains numerous trace elements, such as Al, Ti, Mg, Mn, Zn, Cr, V, Ni, Co and Ga, and can form in a variety of physico-chemical environments. Chemical composition of magnetite thus can be used to fingerprint the types of mineral deposits and to distinguish different ore forming processes (Beaudoin and Dupuis, 2009; Carew, 2004; Chen et al., 2015-in this issue; Dare et al., 2012; Dupuis and Beaudoin, 2011; Hu et al., 2013; Huang et al., 2013, 2014, 2015-in this issue; Müller et al., 2003; Nadoll et al., 2012, 2014; Rusk et al., 2009; Singoyi et al., 2006).

Previous studies of Fe oxides in Bayan Obo have dealt with the paragenesis and chemical compositions of magnetite (IGCAS (Institute of Geochemistry, Chinese Academy of Sciences), 1988; Wei and Shangguan, 1983; Zeng et al., 1981). IGCAS (Institute of Geochemistry, Chinese Academy of Sciences) (1988) identified three generations of magnetite with different mineral assemblages, structures, textures and formation temperatures. Laser spectral analyses showed that different generations of magnetite contain variable amounts of trace elements (IGCAS (Institute of Geochemistry, Chinese Academy of Sciences), 1988; Zeng et al., 1981). However, limited elements were determined due to the poor detection limits of the laser spectral analyses. Therefore, the chemical

* Corresponding author at: State Key Laboratory of Continental Dynamics, Department of Geology, Northwest University, Xi'an 710069, China. Tel.: +86 13037898407.
E-mail address: qilianghku@hotmail.com (L. Qi).

http://dx.doi.org/10.1016/j.oregeorev.2014.09.010
0169-1368/

composition of Fe oxides has not been fully understood and the origin of the Fe oxides remains unconstrained.

In this paper, we describe ore petrography with emphasis on the magnetite-bearing ores of the Bayan Obo deposit. Using in situ laser ablation inductively coupled plasma mass spectrometry (LA-ICP-MS), we obtain trace elemental compositions of the magnetite and hematite from various ore types of the Bayan Obo deposit. The new dataset provides a better understanding of the compositions of ore-forming fluids and processes responsible for Fe and possible REE mineralization. We also compare the compositions of magnetite from the Bayan Obo deposit with other types of mineral deposits.

2. Geological setting

2.1. Regional geology

The Bayan Obo deposit is located in the northern margin of the North China Craton (NCC). To the north of the NCC is the Central Asian Orogenic Belt (CAOB) (Yang et al., 2011) (Fig. 1a). The crystalline basement in this area is represented by the Archean Se'ertengshan complex composed of migmatite, gneiss, granulite, quartz schist, and amphibolite with ages ranging from 2.6 to 1.9 Ga (Fan et al., 2010). The basement is unconformably overlain by the Mesoproterozoic Bayan Obo Group, which consists of coarse- to medium-grained clastic and carbonate rocks, and fine-grained slates (Bai et al., 1996). Cambrian–Ordovician sedimentary rocks are locally distributed to the south and east of the Bayan Obo area. Carboniferous and Permian continental coal-bearing clastic sedimentary sequences are distributed further to the south. Igneous rocks in the area include Proterozoic carbonatite dykes (Fan et al., 2014; Le Bas et al., 1992, 1997; Tao et al., 1998; Wang et al., 2010; Yang et al., 2011), and Permian gabbroic and granitic plutons (Drew et al., 1990; Fan et al., 2009; IGCAS (Institute of Geochemistry, Chinese Academy of Sciences), 1988; Ling et al., 2014; Qiu et al., 2003, 2008, 2011; Zhang et al., 2003).

2.2. Deposit geology

The Bayan Obo deposit has estimated reserves up to 1500 Mt of Fe ore (35 wt.% Fe), 48 Mt REE (6 wt.% RE_2O_3) and 1 Mt Nb (0.13 wt.% Nb) (Wu, 2008). Detailed descriptions of the deposit geology are available in Bai et al. (1996), IGCAS (Institute of Geochemistry, Chinese Academy of Sciences) (1988), Smith and Wu (2013), Smith et al. (2015), and Zhang et al. (1995, 2003) and the geology is only briefly summarized here. The hosting Proterozoic Bayan Obo Group is divided into 18 horizons, including lower nine horizons, numbered from H1 to H9, in the Bayan Obo area (Drew et al., 1990). The lower part of the Bayan Obo Group (H1) is composed of basal conglomerate and is overlain by a sequence of quartzite, carbonaceous slate, sandstone, limestone and siltstone (H2–H7). Orebodies are mainly hosted in dolomite marble (H8) and locally in slate and biotite schist (H9) (Fig. 1b).

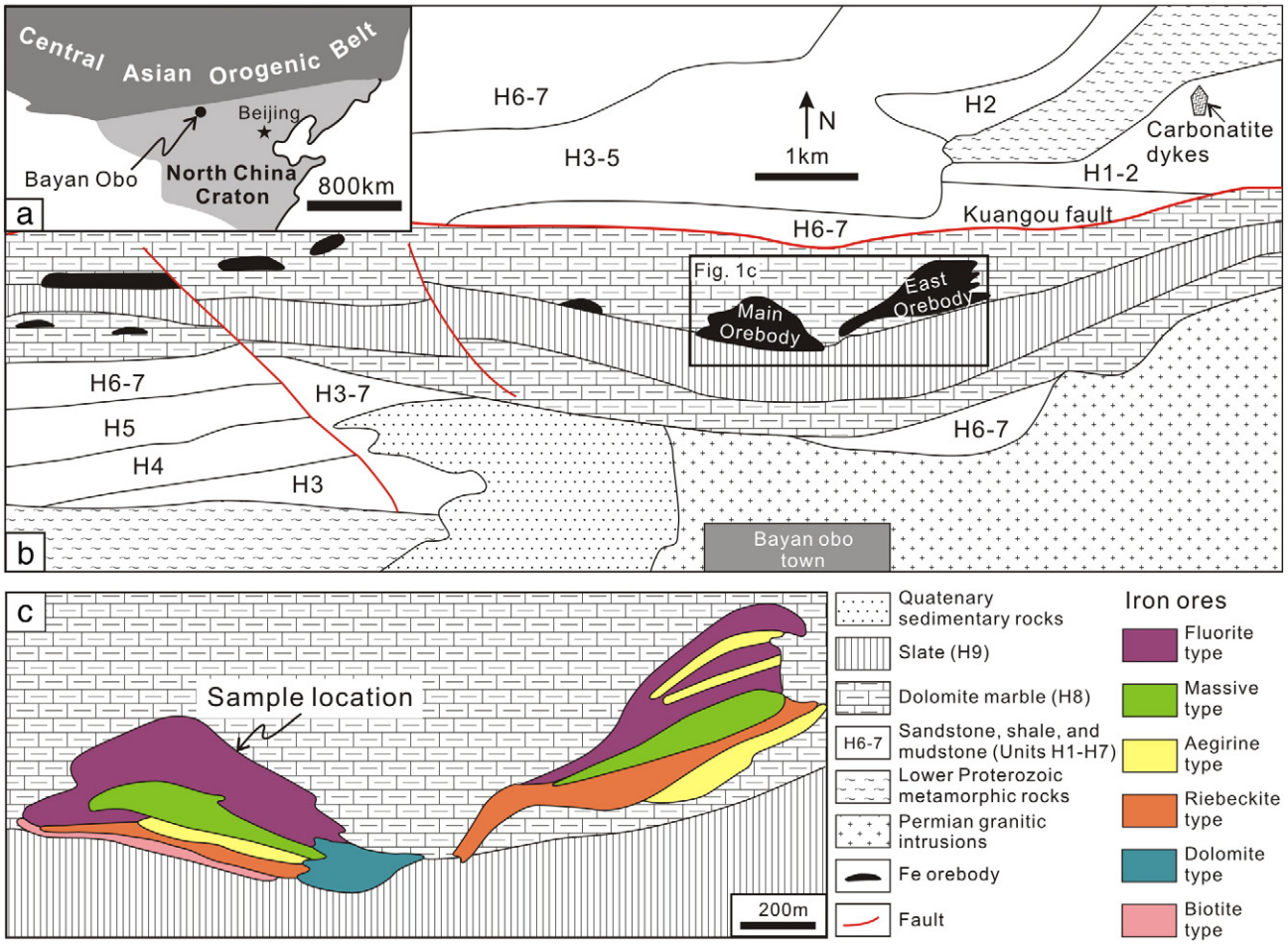

Fig. 1. (a) The tectonic location of the Bayan Obo deposit in the North China Craton (modified from Yang et al., 2011). (b) Simplified geological map of the Bayan Obo deposit (Yang et al., 2009). (c) Distribution of different types of Fe ores of the Main Orebody and East Orebodies (Sun et al., 2013).

Those include the Main Orebody, East Orebody, and several small-scale orebodies in the west (Fig. 1b). The Main Orebody is the largest one in the Bayan Obo. The larger Main Orebody and East Orebody are distributed in the dolomite marble (H8) and are close to the boundary of K-rich slate (H9). These western orebodies are mainly hosted in H8 dolomite marble (Fig. 1b).

There are three major mineralization types, including REE, Fe-oxide, and Nb mineralization. Our work focuses on the Fe-oxide mineralization. The Fe-oxide mineralization is characterized by the ore minerals of magnetite and hematite and associated gangue minerals such as fluorite, aegirine, riebeckite, biotite, dolomite, apatite, barite, pyrite, monazite, and other REE minerals. According to mineral assemblage, the Fe ores are divided into dolomite, fluorite, riebeckite, biotite, and aegirine types (Fig. 1c) (Wei and Shangguan, 1983; Zeng et al., 1981), which show disseminated, banded, and massive structures. The paragenetic sequence of the Fe-oxide mineralization is very complex (Chao et al., 1997; Zeng et al., 1981). Zeng et al. (1981) identified three generations of magnetite based on mineral assemblages, structures, and textures. Chao et al. (1997) considered the formation of hematite was earlier or later than magnetite.

3. Petrography of Fe ores

Six Fe ore samples, including banded, disseminated and massive ores, are selected for this study (Fig. 2). Detailed petrographic observations of these samples were made prior to LA-ICP-MS analyses.

Banded ore samples, B-1, 92-O-99, M-2 and 92-O-137, show different mineral assemblages. The banded aegirine ore (B-1) consists of magnetite, aegirine, biotite, barite and minor apatite and REE minerals (Figs. 2a and 3a). Magnetite was commonly replaced by hematite along the margin (Fig. 4a). The banded barite ore (92-O-99) has magnetite and barite bands (Fig. 2b) and consists of magnetite, barite, apatite, and minor phlogopite and REE minerals (Fig. 3b). Magnetite grains are anhedral to subhedral and are commonly less than 100 μm in diameter (Fig. 4b). The banded fluorite ores (M-2 and 92-O-137) show banded structure (Fig. 2c) and are mainly composed of magnetite and fluorite with minor apatite, dolomite, calcite, aegirine, riebeckite and REE minerals (Fig. 3c–e). REE minerals occur as wide bands that crosscut magnetite grains (Fig. 3c), indicating later formation of REE minerals. Micron-sized REE mineral inclusions are abundant in magnetite grains (Fig. 3d) and were avoided during the analyses. Magnetite grains are anhedral or euhedral (Fig. 4c) and are locally replaced by hematite (Fig. 4d).

The disseminated ore (208-4-1) comprises magnetite and dolomite with minor biotite, barite, oligonite, humite, ilmenite, and REE minerals (Figs. 2d and 3f). Barite occurs as small veins crosscutting magnetite grains, indicating later formation of barite. Magnetite occurs as mineral aggregates (Fig. 4e).

The massive ore (B-2) shows a massive structure (Fig. 2e) composed of magnetite, quartz, aegirine, riebeckite, and minor ilmenite, barite, albite, and REE minerals (Fig. 3g and h). Magnetite was commonly replaced by hematite along the margin (Fig. 4f).

4. Analytical results

Fe oxides, magnetite and hematite, from different types of Fe ores were analyzed for trace elements at the State Key Laboratory of Ore Deposit Geochemistry, Institute of Geochemistry, Chinese Academy of Sciences, using a Coherent GeoLasPro 193 nm Laser Ablation system

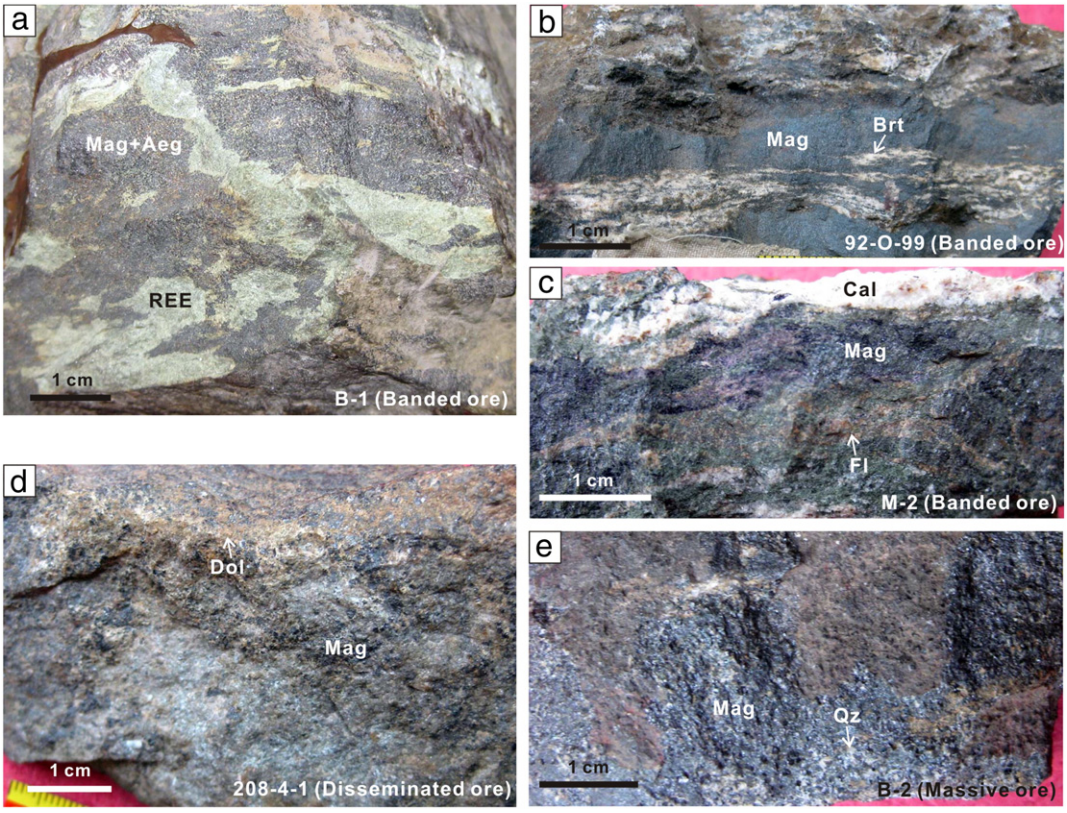

Fig. 2. Photos of Fe-REE ores from the Bayan Obo deposit. (a) Banded ore composed of magnetite, aegirine and REE minerals. (b) Banded ore composed of barite and magnetite. (c) Banded ore comprising magnetite, fluorite, and calcite. (d) Disseminated ore consisting of dolomite and magnetite. (e) Massive ore composed of magnetite and minor quartz. Mag, magnetite; Aeg, aegirine; Fl, fluorite; Cal, calcite; Qz, quartz; Dol, dolomite; REE, REE minerals.

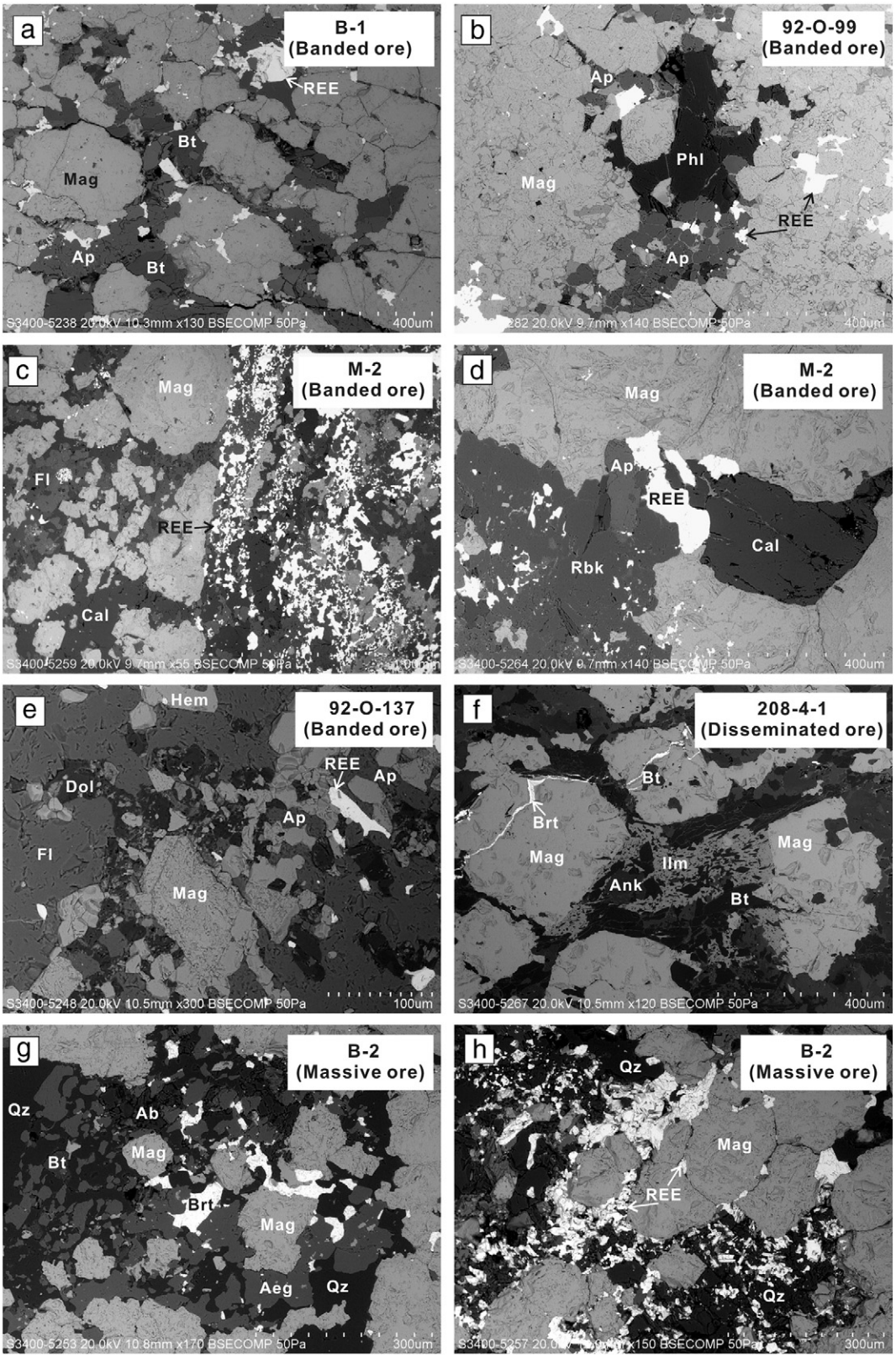

Fig. 3. Back-scattered electron (BSE) micrographs of ores from the Bayan Obo deposit. (a) Subhedral magnetite associated with apatite, biotite, and REE minerals. Some REE minerals infilling the fracture of magnetite grains indicate their later formation. (b) Magnetite associated with apatite, phlogopite, and REE minerals. (c) Anhedral to subhedral magnetite associated with fluorite, calcite, and REE minerals. (d) Magnetite associated with apatite, calcite, riebeckite, and REE minerals. (e) Magnetite associated with apatite, fluorite, dolomite, and REE minerals and replaced by hematite. (f) Magnetite associated with ilmenite, biotite, and dolomite. Magnetite grains were crosscut by small barite veins, indicating the later formation of barite. (g) Magnetite associated with aegirine, quartz, biotite, barite, and albite. (h) The fracture of magnetite infilled by REE minerals indicates earlier formation of magnetite. Dol, dolomite; Mag, magnetite; Brt, barite; Ab, albite; Aeg, aegirine; Ap, apatite; Phl, phlogopite; Bt, biotite; Fl, fluorite; Qz, quartz; Cal, calcite; Dol, dolomite; Rbk, riebeckite; Ilm, ilmenite; Hem, hematite. REE, REE minerals.

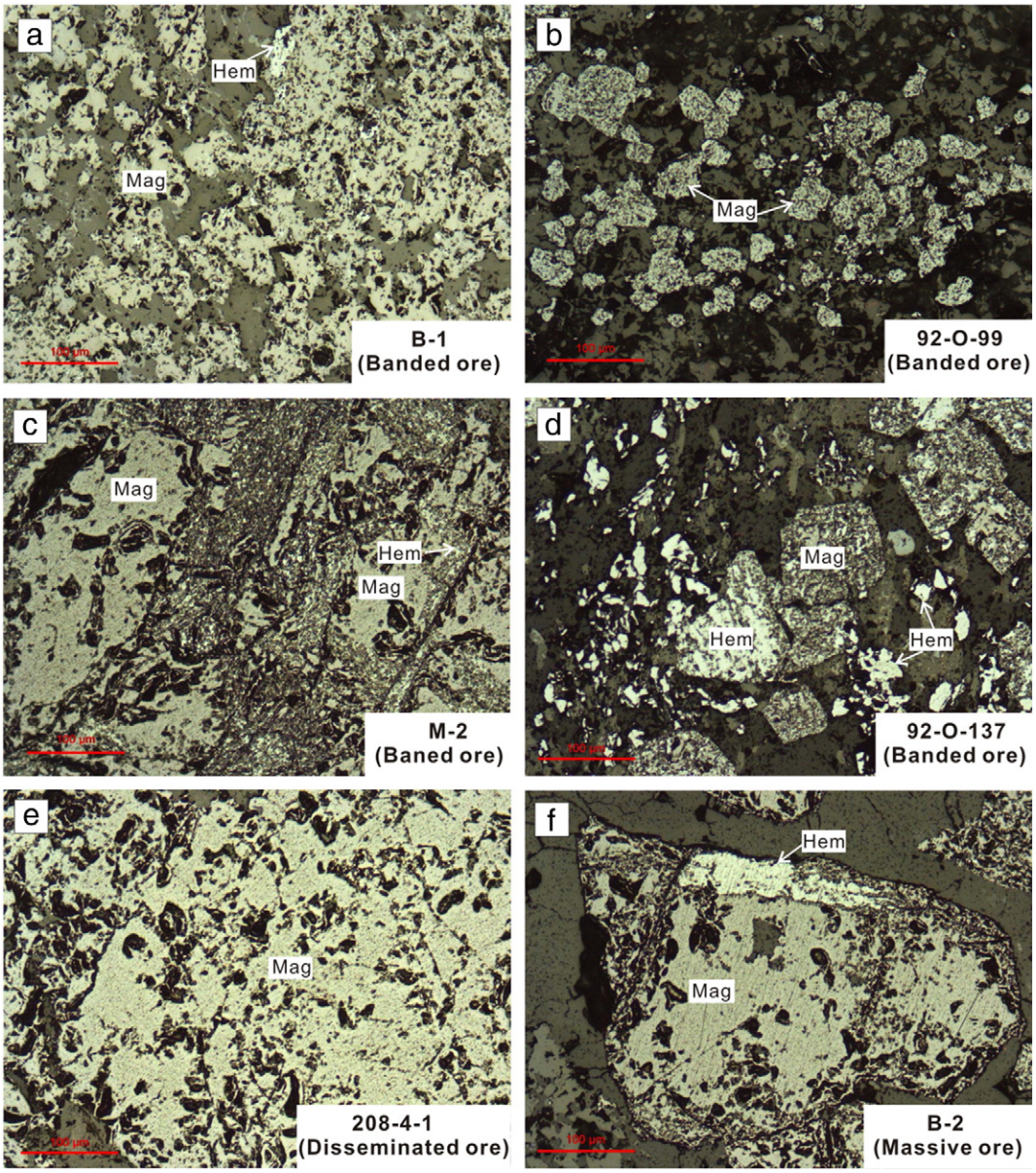

Fig. 4. Photomicrographs of Fe ores (under reflected light). (a) Magnetite from the banded ore occurs as anhedral crystal and was commonly replaced by hematite. (b) Magnetite grains from the banded ore occur as subhedral crystals that are smaller than 100 μm in diameter. (c) Magnetite replaced by hematite along the fracture of magnetite. (d) Euhedral magnetite from the banded ore replaced by hematite. (e) Disseminated ore composed of magnetite aggregates. (f) Magnetite aggregates replaced by hematite along the margin. Mag, magnetite; Hem, hematite.

coupled with an Agilent 7700x ICP-MS. Analytical methods are available in Gao et al. (2013), Huang et al. (2013), and Liu et al. (2015-in this issue).

A total of 51 elements, including 14 rare earth elements, were analyzed for magnetite and hematite. Sodium, Si, P, K, Ca, Cu, Ge, Rb, Zr, Ag, Cd, In, Lu, Hf, W, Th, and U are either close to or below the detection limit or showing considerable variation in contents and are not used in this study. The mean contents and standard deviation of the selected major and trace elements of Fe oxides from different types of ores are listed in Table 1. All the results are given in Appendix 1.

Magnetite grains from the Bayan Obo contain variable concentrations of trace elements. They have ~30–1000 ppm Mg, ~2–100 ppm Al, ~300–10000 ppm Mn, ~40–400 ppm V, 5–1000 ppm Ti, and ~5–100 ppm Cr (Table 1). Inter-element relationships for magnetite grains from all types of ores are examined in binary plots (Fig. 5). Magnesium shows a positive correlation with Al for banded fluorite and disseminated ores (Fig. 5a). There are no obvious correlations between V vs. Ti, and V vs. Cr (Fig. 5b and c) due to relatively constant V contents for magnetite from all types of ores. In the plots of Mn vs. Co and Mn vs. total REE, magnetite grains from three types of ores define three separated fields due to different Mn and REE contents (Fig. 5d and e). Lead shows a weakly positive correlation with Zn for magnetite grains from the disseminated ore (Fig. 5f). Magnetite from the banded fluorite ore (92-O-137) has the highest Zn contents, whereas that from the banded aegirine ore has the lowest Zn contents (Fig. 5f). Those from the banded barite ore have the highest Nb and Y contents (Fig. 5g). Niobium shows a weakly positive correlation with Y for magnetite grains from the banded and disseminated ores (Fig. 5g). Lead shows an obviously positive correlation with Bi for magnetite grains from the banded ores (Fig. 5h).

Table 1
Summary of LA-ICP-MS results for trace elements (in ppm) in iron oxides from the Bayan Obo Fe-REE-Nb deposit.

Sample no.	D.L.	M-2		B-1		92-O-137				92-O-99		208-4-1		B-2			
Ore type		Banded type		Banded type		Banded type				Banded type		Disseminated type		Massive type			
Fe oxides		Mag		Mag		Mag		Hem		Mag		Mag		Hem		Mag	
		ave (n = 21)	stdev	ave (n = 14)	stdev	ave (n = 9)	stdev	ave (n = 9)	stdev	ave (n = 12)	stdev	ave (n = 11)	stdev	ave (n = 7)	stdev	ave (n = 14)	stdev
Mg	2.63	137	89	168	86	59.1	27.4	44.6	18.6	102.1	28.4	1430	274	90.4	17.2	81.5	16.6
Al	4.69	20.4	6.0	39.4	27.2	47.5	24.1	18.0	5.3	92.6	16.1	11.6	6.6	14.1	3.4	16.7	4.9
Sc	1.18	1.67	0.69	5.27	2.6	11.9	10.7	4.09	3.86	10.3	4.2	3.40	1.55	1.97	0.30	1.84	0.40
Ti	0.972	367	168	221	33	20.4	12.2	19.1	10.2	57.3	28.1	552	121	93.8	30.9	80.9	18.7
V	0.306	110	10	53.0	4.2	118	8	115	6	364	15	92.8	3.8	375	28	357	21
Cr	2.84	24.4	11.5	19.0	15.9	41.7	12.7	20.8	14.9	109	24	11.1	4.4	61.7	48.8	81.3	56.3
Mn	7.67	604	64	1268	67	413	82	357	36	942	131	8569	552	2128	77	2213	59
Co	0.135	4.86	1.25	5.67	1.20	20.0	2.8	19.4	2.3	70.0	3.3	23.6	2.8	11.9	1.2	11.8	1.7
Ni	8.35	51.3	14.1	41.7	22.0	172	18	165	24	177	20	38.4	20.4	69.8	33.7	66.9	37.0
Zn	4.42	267	25	99.4	19.4	1633	105	1601	99	225	27	304	35	248	47	219	29
Ga	0.055	3.36	0.95	2.02	0.70	2.65	0.94	2.69	1.07	1.05	0.59	0.81	0.27	5.76	0.86	4.51	1.17
Sr	<0.001	1.10	1.07	2.59	2.95	2.70	3.55	1.14	1.76	10.5	4.7	0.924	1.833	0.473	0.150	0.150	0.087
Y	<0.001	0.522	0.402	0.973	1.084	1.23	0.88	0.898	0.749	11.3	4.7	0.237	0.152	0.583	0.799	0.496	0.393
Nb	0.03	26.5	49.8	3.34	2.37	15.5	15.2	15.8	20.5	415	67	19.4	15.0	54.1	64.4	1.36	1.95
Mo	<0.001	1.53	1.36	1.79	1.48	9.58	8.8	1.91	2.13	8.82	2.69	0.426	0.140	0.597	0.322	0.385	0.223
Sn	0.872	6.57	2.51	1.09	0.14	1.99	0.5	1.25	0.11	3.36	1.23	55.2	4.4	1.79	0.86	1.42	0.54
Ba	<0.001	11.4	6.9	10.8	5.1	4.11	4.17	1.90	1.31	41.9	25.6	2.18	1.49	1.89	1.79	4.40	7.36
Pb	0.037	6.13	6.21	4.31	5.14	16.8	18.5	2.87	2.86	134	28	1.50	1.87	3.91	4.62	0.415	0.291
Bi	0.012	0.500	0.400	0.628	0.831	5.87	6.37	0.610	0.460	3.65	1.26	0.068	0.023	0.137	0.072	0.036	0.018
La	0.008	1.96	1.18	2.84	3.25	0.359	0.352	0.549	0.734	4.23	1.83	0.044	0.028	0.260	0.291	0.330	0.795
Ce	0.012	9.79	6.35	13.6	16.3	2.19	2.14	1.99	3.02	9.75	2.01	0.178	0.173	0.766	0.831	0.678	1.56
Pr	0.002	1.46	0.936	2.27	2.52	0.410	0.360	0.254	0.264	2.06	0.737	0.091	0.038	0.158	0.168	0.099	0.171
Nd	<0.001	4.82	3.15	9.62	10.4	1.34	1.50	1.03	1.01	11.7	4.16	0.394	0.301	0.591	0.682	0.500	0.951
Sm	0.011	0.585	0.322	1.03	0.876	0.346	0.182	0.335	0.305	4.13	0.925	0.192	0.140	0.413	0.213	0.203	0.160
Eu	0.002	0.122	0.085	0.192	0.183	0.064	0.066	0.032	0.036	1.49	0.373	0.036	0.030	0.043	0.057	0.027	0.031
Gd	0.010	0.183	0.113	0.444	0.423	0.336	0.313	0.130	0.062	3.92	0.950	0.104	0.026	0.249	0.289	0.105	0.044
Tb	0.002	0.026	0.018	0.090	0.142	0.051	0.021	0.039	0.033	0.753	0.212	0.013	0.009	0.102	0.103	0.021	0.007
Dy	0.009	0.143	0.097	0.263	0.267	0.299	0.288	0.303	0.388	4.92	1.45	0.097	0.055	0.263	0.201	0.197	0.139
Ho	<0.001	0.037	0.037	0.055	0.048	0.093	0.100	0.090	0.065	0.793	0.300	0.013	0.006	0.056	0.049	0.038	0.028
Er	0.004	0.099	0.086	0.139	0.150	0.347	0.369	0.240	0.239	1.93	0.711	0.065	0.052	0.125	0.000	0.092	0.086
Tm	0.003	0.015	0.007	0.024	0.019	0.022	0.021	0.034	0.018	0.203	0.083	0.015	0.008	0.031	0.013	0.031	0.008
Yb	<0.001	0.062	0.061	0.087	0.090	0.169	0.123	0.151	0.102	1.06	0.563	0.061	0.024	0.093	0.067	0.095	0.071
Lu	0.002	0.013	0.014	0.018	0.011	0.026	0.016	0.017	0.011	0.105	0.080	0.011	0.004	0.012	0.000	0.036	0.034
∑REE		19.3		30.6		6.05		5.20		47.1		1.31		3.16		2.45	
$(La/Yb)_N$		21.3		22.0		1.44		2.46		2.70		0.49		1.89		2.35	
$(Gd/Yb)_N$		2.39		4.14		1.61		0.70		3.01		1.38		2.17		0.90	
$(La/Sm)_N$		2.10		1.73		0.65		1.03		0.65		0.14		0.40		1.02	

Abbreviation: D.L. = detection limit, ave = average, stdev = standard deviation, Mag = magnetite, Hem = hematite.
Detection limit (D.L.) = $3 \times \sigma^i_{background} \times C^i_{RM}/cps^i_{RM}$, where $\sigma^i_{background}$ is the standard deviation of multiple determinations of element *i* in the background, C^i_{RM} and cps^i_{RM} are concentration and peak intensity of element *i* in the reference material, respectively.
REE contents of chondrite for normalization are from Taylor and McLennan (1985).

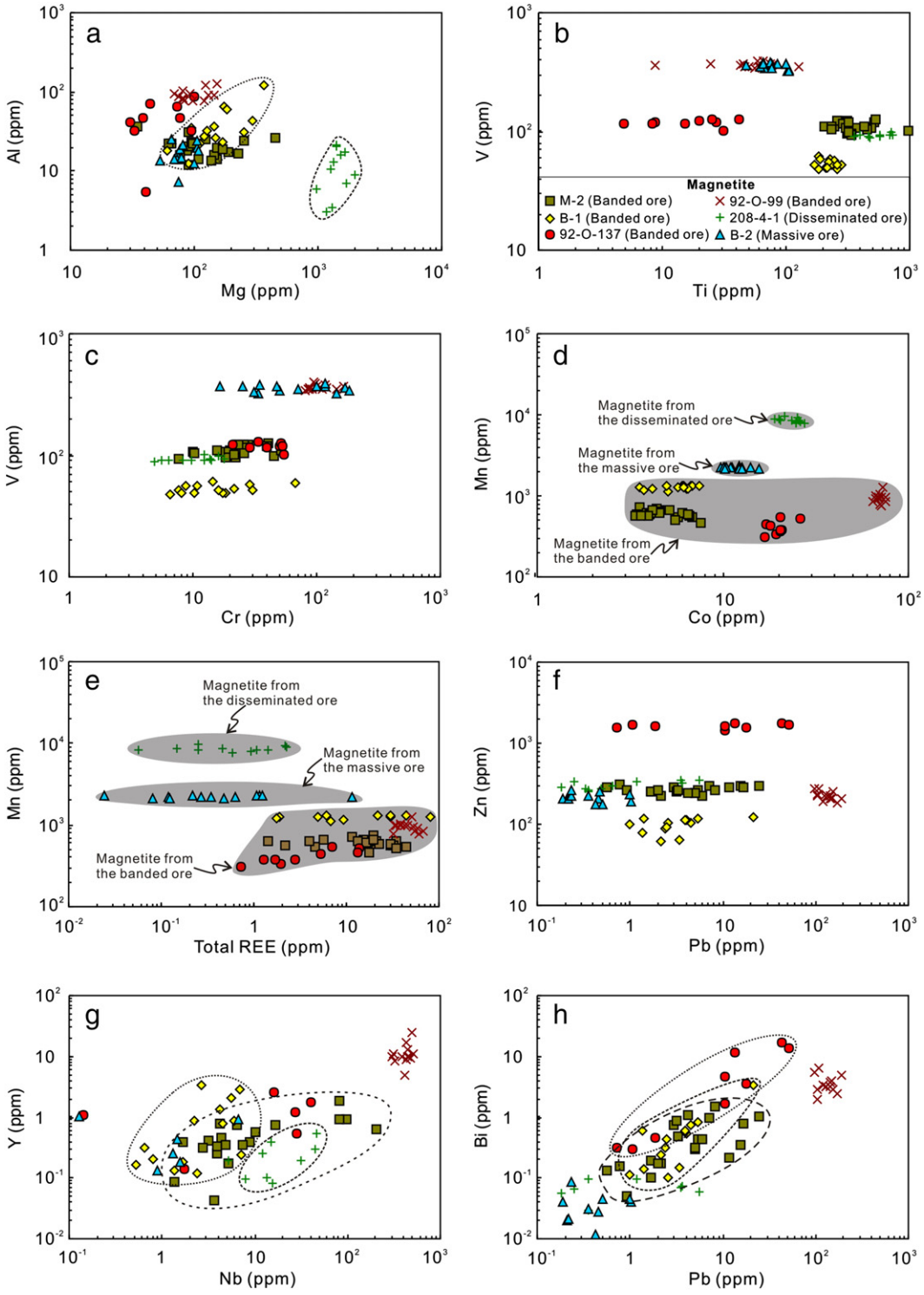

Fig. 5. Bi-plots of selected trace elements of magnetite from different types of Fe ores from the Bayan Obo deposit.

In general, trace element contents of magnetite from different types of Fe ores vary less than two orders of magnitude (Fig. 6a). Magnetite grains from the banded barite ore (92-O-99) and the disseminated ore (208-4-1) have trace element patterns different from other types of Fe ores. Magnetite grains from the banded barite ore have the highest Al, Sc, V, Cr, Co, Sr, Y, Nb, Mo, Ba, Pb, and Bi, whereas those from the disseminated ore contain the highest Mg, Ti, Mn, and Mo (Fig. 6a). Hematite and magnetite from the same ore sample have similar Mg, Ti, V, Mn, Co, Ni, Zn, Ga, Sn, and Ba (Fig. 6b).

Total REE contents of magnetite grains from all types of ores range from 1.31 to 47.1 ppm, whereas those of hematite range from 3.16 to 5.20 ppm (Table 1). Magnetite grains from the banded ores with different mineral assemblages have different REE patterns (Fig. 7a). Magnetite grains from the banded barite ore have the

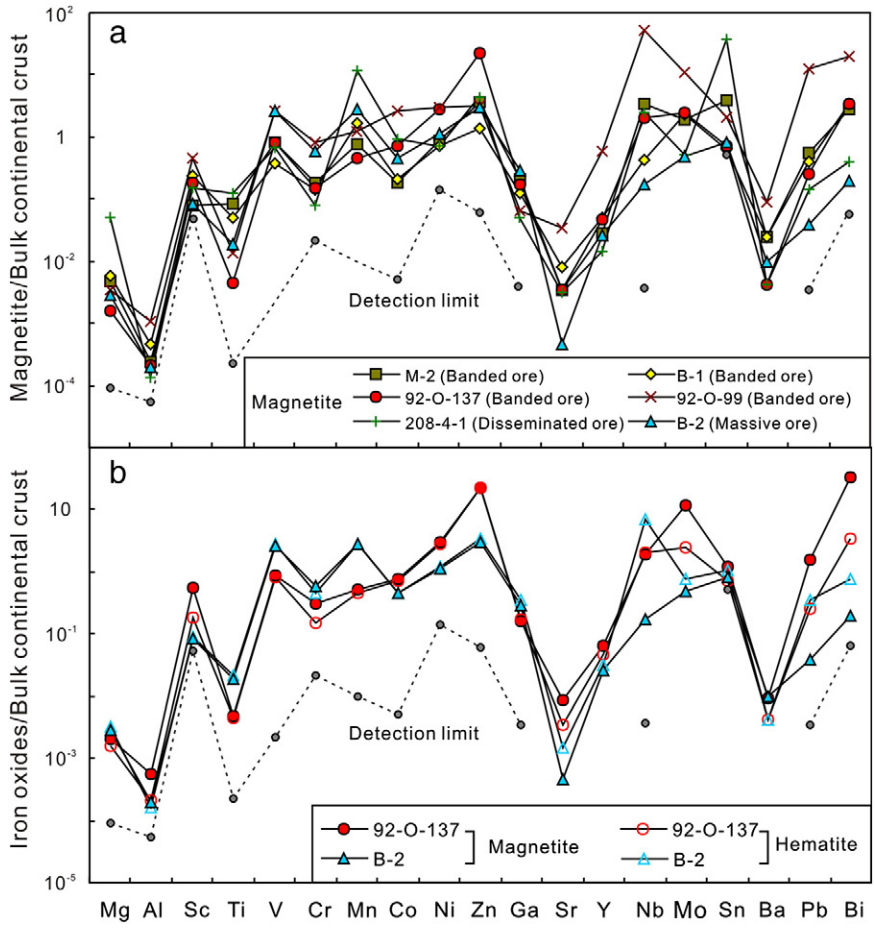

Fig. 6. Bulk continental crust normalized trace element patterns of (a) magnetite from different types of ores, and (b) magnetite and hematite from the same ores. Trace element contents of bulk continental crust are from Rudnick and Gao (2003).

highest total REE content of 47.1 ppm with light-REE and middle-REE enrichment ($(La/Yb)_N = 2.70$, $(Gd/Yb)_N = 3.01$), whereas those from other banded ores have total REE contents ranging from 6.05 to 30.6 ppm and are rich in light REEs with $(La/Yb)_N$ values of ~1.4–22 (Table 1 and Fig. 7a). The massive and disseminated ores have lower total REE contents ranging from 1.31 to 2.45 ppm, which show no or weakly light-REE enrichment with $(La/Yb)_N$ values ranging from 0.49 to 2.35 (Table 1 and Fig. 7a). Hematite has similar total REE contents and REE patterns to the associated magnetite from the same ore sample (Fig. 7b).

5. Discussion

Previous studies have demonstrated that there are at least three generations of magnetite (IGCAS (Institute of Geochemistry, Chinese Academy of Sciences), 1988; Wei and Shangguan, 1983; Zeng et al., 1981). Magnetite of the first generation was thought to be sedimentary in origin and was closely associated with dolomite, quartz, biotite, alkaline amphibole, bastnaesite, and monazite. Magnetite of the second generation was considered to have formed by metamorphism from sedimentary magnetite overprinted by hydrothermal processes. Magnetite in the third generation was considered to be magmatic-hydrothermal in origin and formed by the contact metasomatism between dolomite and Late Paleozoic granitic rocks. Magnetite of this generation was associated with magnesium skarn minerals and has characterized exsolution textures. Magnetite from this study formed in two generations which correspond to the first and second generation as described in IGCAS (Institute of Geochemistry, Chinese Academy of Sciences) (1988). Skarn magnetite is not considered in this study. Trace elemental compositions of Fe oxides provides further evidence of the origins of different generations of magnetite and thus have significant implications for multiple origins of the Fe mineralization at Bayan Obo.

5.1. Sedimentary magnetite

Banded ores have magnetite bands and aegirine/fluorite/barite/REE mineral bands, as typical sedimentary structures (Fig. 2a–c). Oolitic stromatolites were also previously reported in these banded ores (IGCAS (Institute of Geochemistry, Chinese Academy of Sciences), 1988). In the field, the banded ores are commonly intercalated with quartzite. These ores may represent a sedimentary package resembling banded iron formation (BIF).

Magnetite grains from all banded ores plot in the BIF and extended BIF fields (Fig. 8a), indicating their similar origins. Magnetite grains from the banded ores, M-2, B-1 and 92-O-99, plot in the center or margin of the BIF field defined by Dupuis and Beaudoin (2011), on an X–Y plot, whereas those from the banded ore, 92-O-137, plot in the extended BIF field defined by Nadoll et al. (2014) and Chung et al. (2015-in this issue) (Fig. 8a). The geochemical affinity of magnetite with BIFs indicates the derivation of magnetite from a sedimentary process. The existence of hydrothermal minerals in banded ores indicates that the ores may have experienced hydrothermal process. Sedimentary (metamorphic) magnetite in unaltered BIFs rarely contains more than 10 ppm Co and 50 ppm Ni with Co/Ni ratios ranging from 0.1 to 1, whereas hydrothermal magnetite in low grade metamorphic hematite–chert BIFs have average Co and Ni concentrations in excess of 500 and

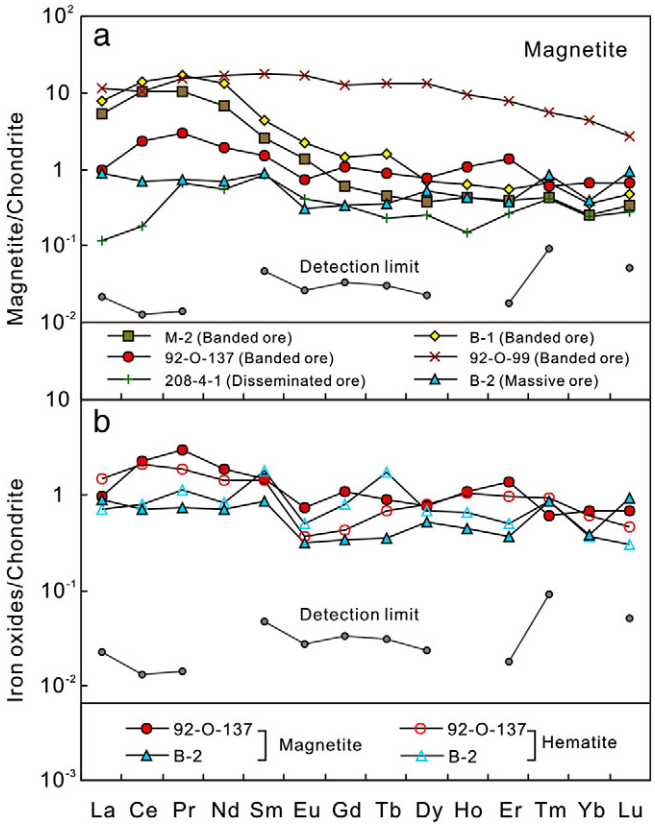

Fig. 7. Chondrite-normalized rare-earth-element patterns of (a) magnetite from different types of ores, and (b) magnetite and hematite from the same ores. Normalization values are from Taylor and McLennan (1985).

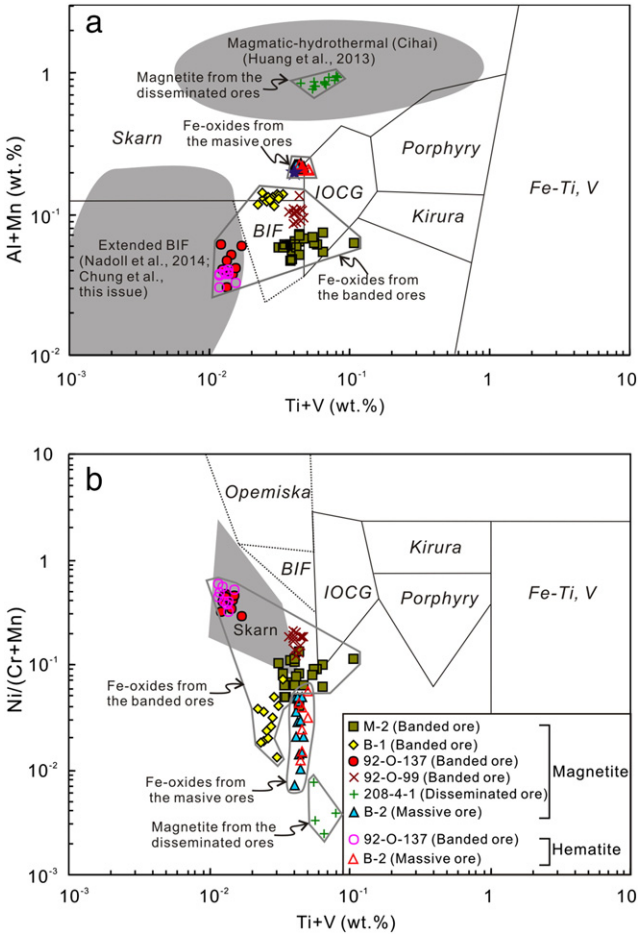

Fig. 8. Plots of Al + Mn vs. Ti + V (a) and Ni/(Cr + Mn) vs. Ti + V (b) for LA-ICP-MS data of Fe oxides from the Bayan Obo deposit. Because Ca content of Fe oxides (<100 ppm) is lower than the detection limit (~500 ppm), Ca content is calculated using zero ppm. Reference fields are after Dupuis and Beaudoin (2011). The pentagram represents the average composition of magnetite grains from the Bayan Obo which was reported by Dupuis and Beaudoin (2011). *BIF*, banded iron formation; *Skarn*, Fe–Cu skarn deposits; *IOCG*, iron oxide–copper–gold deposits; *Porphyry*, porphyry Cu deposits; *Kiruna*, Kiruna apatite–magnetite deposits; *Fe-Ti, V* magmatic Fe–Ti-oxide deposits.

350 ppm, respectively, with Co/Ni ratios greater than 1 (Nadoll et al., 2014). Magnetite grains in the BIF field have less than 100 ppm Co and 200 ppm Ni with Co/Ni ratios of ~0.1, indicating that the compositions of these magnetite grains were not significantly altered from hydrothermal modification.

5.2. Metasomatic magnetite and possible fluid composition

Magnetite of this generation is characterized by metasomatic textures (Fig. 4f) and was typically associated with fluorite, aegirine, and alkaline amphibole. It is likely that magnetite in the disseminated and massive ores belongs to this generation corresponding to the second generation of IGCAS (Institute of Geochemistry, Chinese Academy of Sciences) (1988). Magnetite grains of the second generation show slightly different normalized trace element patterns from those of the first generation (Fig. 6a), as well as higher Mg and Mn contents (Fig. 5a, d and e), indicating their different origins. Magnetite grains of the second generation plot in the skarn and magmatic-hydrothermal fields (Fig. 8a), also indicating their derivation from different origins from the banded ores. This conclusion is supported by different Ni/(Cr + Mn) values of magnetite grains of different generations as shown in Fig. 8b.

Magnetite grains of the second generation have Mg contents similar to that of the magmatic-hydrothermal deposits, such as the Cihai Fe deposit in NW China (Huang et al., 2013). These grains have significantly higher Mn (7754–9566 ppm) than those of skarn deposit (Dupuis and Beaudoin, 2011) and magmatic-hydrothermal deposit (Huang et al., 2013). These grains are plotted in the field of skarn and magmatic-hydrothermal fields due to the elevated Mg and Mn contents of (Fig. 8a) (Dupuis and Beaudoin, 2011; Huang et al., 2013; Zhao and Zhou, 2015-in this issue). These results are consistent with those of Dupuis and Beaudoin (2011) such that Fe-oxide minerals from the Bayan Obo deposit plot in the field of the skarn type deposits, very close to the field of IOCG deposits (Fig. 8a) and have Ni contents too low to be plotted in Fig. 8b. The low Ni/(Cr + Mn) values of magnetite from this study resulted from high Mn contents rather than low Ni contents. The geochemical affinity of magnetite from the Bayan Obo with that from the hydrothermal deposits indicates their hydrothermal origin.

Magnetite grains from the massive and disseminated ores have similar trace element contents with slightly different chondrite-normalized REE patterns (Fig. 7a). Single dolomite grains have LREE contents ranging from 10 to more than 3000 times chondritic values and shows the REE patterns and Fe contents changing dramatically from MREE-enriched in the center to LREE-enriched near the rim, which was explained by hydrothermal metasomatism of carbonate by REE and Fe-enriched fluids (Ling et al., 2013). Therefore, the slightly different REE patterns between magnetite grains from the disseminated and massive ores may reflect variable process of fluid metasomatism.

It has been demonstrated that the composition of metasomatic magnetite was controlled by fluid compositions, host rock and fluid/rock interaction (Nadoll et al., 2014). For example, in skarn systems

Mg and Mn can successively be enriched in hydrothermal fluids by extensive fluid/rock interactions (e.g. Baker et al., 2004; Einaudi et al., 1981; Meinert, 1992; Nadoll et al., 2014). Therefore, magnetite containing elevated Mg and Mn was most likely formed by metasomatism of the host dolomite by Mn-rich hydrothermal fluids. However, Mn enrichment by the formation of massive magnetite cannot be excluded, because this process would lead to strong enrichment of Mn relative to Fe in the remaining hydrothermal fluid (Ilton and Eugster, 1989; Zhao and Zhou, 2015-in this issue). Magnetite and hematite grains from the same ores have similar trace element contents and REE patterns, indicating their derivation from the same ore fluids. This conclusion is consistent with previous studies (Dupuis and Beaudoin, 2011; Nadoll et al., 2014; Zhang et al., 2011).

5.3. Implications for the REE mineralization

Magnetite and REE minerals of the Bayan Obo deposit were considered to have multiple generations and thus multiple origins (Chao et al., 1995; Fang and Qiu, 1997; IGCAS (Institute of Geochemistry, Chinese Academy of Sciences), 1988; Kynicky et al., 2012; Wei and Shangguan, 1983; Zeng et al., 1981). Fe and REEs were suggested to be derived from terrigenous sediments and deep stratigraphic basinal brine (Fang et al., 1995; Hou, 1989; Meng, 1982; Meng and Drew, 1992; Tu, 1998; Xiao et al., 2003; Yang and Drew, 1994). Fe and REEs were also considered to have formed by hydrothermal replacement of Proterozoic sedimentary dolomite (Campbell and Henderson, 1997; Cao et al., 1994; Chao et al., 1992, 1997; Drew et al., 1990; Ling et al., 2013; Smith et al., 2000; Yang et al., 2009). The hydrothermal fluids were possibly derived from alkaline–carbonatite intrusive rocks (Drew et al., 1990), carbonatite (Campbell and Henderson, 1997; Ling et al., 2013; Yang et al., 2009), or both carbonatite and granite (Cao et al., 1994).

Magnetite grains from the banded ores show similar bulk continental crust-normalized trace element and chondrite-normalized REE patterns (Figs. 6a and 7a), indicating derivation from the same ore-forming fluids. Magnetite grains from the banded barite ore show trace element and REE patterns obviously different from those of other types (Figs. 6a and 7a), indicating that these magnetite grains may have different origins. Therefore, there are at least two stages of REE mineralization associated with Fe mineralization. The first stage of REE mineralization was related to a sedimentary process. Magnetite grains of this stage have high total REE contents and show slightly LREE and MREE enrichment. REEs at the second stage were formed by a hydrothermal process. Magnetite grains of this stage have lower REE contents and are obviously LREE enriched.

Due to low partition coefficients of REEs between magnetite and silicate melt, REE contents of magnetite are commonly below the detection limits. For example, the average partition coefficients of Lu, Gd and Y in magmatic systems are 0.15, 0.031 and 0.026, respectively (Dare et al., 2012). Niobium also has a low magnetite–silicate melt partition coefficient of 0.13 (Dare et al., 2012). Similarly, REEs and Nb in hydrothermal systems also rarely partition into magnetite. Therefore, even minor REE and Nb in magnetite also indicates elevated contents of these elements in the ore-forming fluids. The good correlation between Nb and Y of magnetite from the banded and disseminated ores (Fig. 5g) indicates that Nb mineralization may be synchronous with a REE mineralization for these ores. Thus, there are at least two generations of magnetite and two stages of REE mineralization. The first generation of magnetite was represented by the REE-rich banded ores, whereas the second generation of magnetite is hosted in massive and disseminated ores that contain REE minerals and REE-poor magnetite. As illustrated in Fig. 9, with increased hydrothermal metasomatism, REEs in banded ores were leached and were transported by ore fluids, resulting in the formation of REE-poor magnetite and REE minerals.

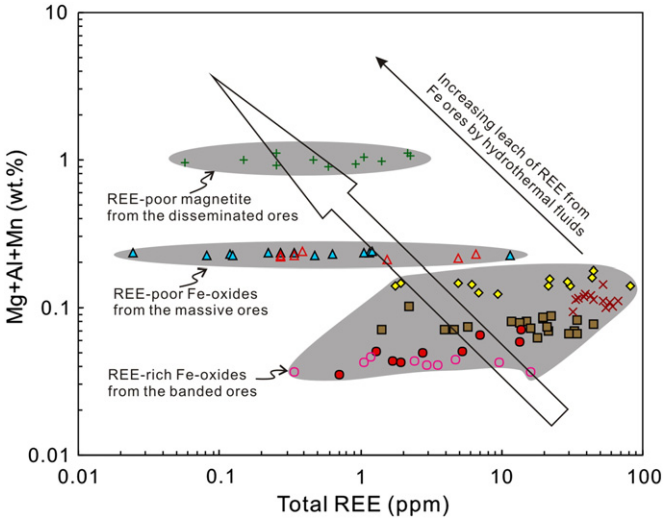

Fig. 9. Plot of Mg + Al + Mn vs. total REE showing the process of Fe and REE mineralization. The symbols are the same as Fig. 8. Magnetite grains from the banded ores have lower Mg + Al + Mn contents and higher REE contents, whereas those from the disseminated and massive ores have higher Mg + Al + Mn contents and lower REE contents. With the increasing hydrothermal metasomatism, REE were leached from the REE-rich banded ores into the ore fluids, resulting in the formation of REE-poor magnetite and REE minerals in disseminated and massive ores.

The hydrothermal metasomatic origin of REE mineralization was also supported by a few zoned zircon grains from the Eastern Orebody (Campbell et al., 2014). These euhedral zircons have potentially magmatic cores, with skeletal rims intergrown with bastnäsite, and have SHRIMP Th-Pb ages of 1325 Ma for zircon cores and 456 Ma for zircon rims. The U-depleted, but Hf and HREE-enriched, zircon cores are similar to those of carbonatitic zircons, whereas the zircon rims are also extremely depleted in U and are intergrown with LREE ore phases and altered by Na and P bearing fluids (Campbell et al., 2014). The highly restricted occurrence of these zircons at the Bayan Obo indicates that they may be produced by a small intrusive body that was subsequently almost obliterated by fluid and tectonic processes. REEs, particularly LREE, were further enriched by fluid metasomatism of the sedimentary carbonate rocks, carbonatite, or already formed Fe ores.

6. Conclusions

Two generations of magnetite from Fe ores of the Bayan Obo deposit have different trace element contents and have different origins. Magnetite of the first generation was sedimentary in origin and is rich in REEs, whereas that of the second generation was hydrothermal in origin and is relatively poor in REEs. The Bayan Obo REE deposit was most likely formed by further enrichment of REEs from REE-rich sedimentary carbonate rocks by metasomatism of hydrothermal fluids.

Acknowledgments

This work was jointly supported by grants from the Chinese 973 project (2012CB416804), the 12th Five-Year Plan Project (SKLODG-ZY125-09), the "CAS Hundred Talents" Project (KZCX2–YW–BR–09) of the Chinese Academy of Sciences, the CAS/SAFEA International Partnership Program for Creative Research Teams (Intraplate Mineralization Research Team, KZZD-EW-TZ-20). We thank Dr. Dai Zhihui for her assistance with LA-ICP-MS analyses at IGCAS (Guiyang). We greatly appreciate two anonymous reviewers for their constructive comments and suggestions and Prof. Franco Pirajno and Prof. Rucheng Wang for effective editorial handling.

Appendix 1. Full analytical results (in ppm) for laser ablation ICP-MS of Fe oxides from the Bayan Obo deposit, North China

Lab no.	Mineral	Sample no.	Mg	Al	Sc	Ti	V	Cr	Mn	Co	Ni	Zn	Ga	Sr	Y	Nb	Mo	Sn
		Detection limit	2.63	4.69	1.18	0.972	0.306	2.84	7.67	0.135	8.35	4.42	0.055	<0.001	<0.001	0.03	<0.001	0.872
13D14A07	Magnetite	M-2-01	225	16.7		519	121	27.8	537	5.71	56.9	287	2.53	1.64	0.557	10.1		7.03
13D14A09	Magnetite	M-2-03	153	14.4		260	124	26	544	6.88	38.5	250	3.02	1.38	0.384	1.71	0.235	3.94
13D14A10	Magnetite	M-2-04	447	26.7	2.86	203	110	20.1	558	6.64	60.5	310	2.01	1.16	0.41	3.21		6.96
13D14A11	Magnetite	M-2-05	65.7	22.6		310	124	22.5	628	6.01	52.9	282	1.75	0.3	0.259	3.91		10.6
13D14A12	Magnetite	M-2-06	86.9	18.2	1.66	243	111	20.9	587	6.44	30.1	301	3.81	0.37	0.747	16.7	1.03	6.7
13D14A14	Magnetite	M-2-07	143	15.7		256	124	23.4	465	7.58	54.1	259	3.39	3.42	0.74	6.45	0.229	3.64
13D14A15	Magnetite	M-2-08	124	24.8	1.19	363	107	19.1	655	4.54	42.4	261	2.18	0.34	0.171	5.28	2.39	6.22
13D14A17	Magnetite	M-2-10	91	20.2	1.32	341	96.1	22.1	704	4.43	31.5	269	2.9	0.37	0.466	4.44	0.525	5.89
13D14A18	Magnetite	M-2-11	61.3	22.3		314	95	18.2	629	4.47	41.2	258	3.98	0.13	0.042	3.6	0.476	4.97
13D14A20	Magnetite	M-2-13	95	23.3		525	125	41	731	3.54	47.2	223	3.91	0.26	0.389	8.69		4.55
13D14A21	Magnetite	M-2-14	109	14		970	101	21.3	622	3.88	74.1	243	2.82	0.26	0.348	7.39	0.497	8.2
13D14A23	Magnetite	M-2-15	251	24		484	108	10.1	597	3.46	55.9	240	3.82	0.44	0.771	4.2	3.99	5.05
13D14A24	Magnetite	M-2-16	89.9	30.4		457	105	10.4	603	4.04	55.7	269	3.6	0.5	0.357	4.89	0.204	8.21
13D14A25	Magnetite	M-2-17	188	17.3		289	115	27.6	625	4.58	70.5	225	4.66	1.34	0.315	2.72		4.52
13D14A26	Magnetite	M-2-18	152	19.3		302	108	16.4	624	4.09	72.9	252	2.78	0.55	0.085	1.38	0.72	3.86
13D14A27	Magnetite	M-2-19	168	18.9		433	109	15.5	671	5.16	54.4	259	3.09	1.03	0.258	3.89		5.59
13D14A28	Magnetite	M-2-20	34.4	36.6		341	92.8	7.68	670	4.2	27.5	248	5.12	0.25	0.334	3.93	1.17	6.03
13D14A40	Magnetite	M-2-31	96.9	22		320	100	45.6	570	3.37	47.2	294	4.84	4.09	0.621	201	2.94	14.1
13D14A41	Magnetite	M-2-32	88.8	12.1		235	109	51.6	573	3.96	39.8	297	3.44	1.39	1.896	82.5	1.55	7.75
13D14A42	Magnetite	M-2-33	76.2	15.7	1.31	232	104	26	578	3.64	50.2	291	2.29	1.65	0.908	97.6	3.14	9
13D14A44	Magnetite	M-2-35	139	13.6		319	119	39.3	511	5.52	74.4	287	4.55	2.19	0.909	82.4	3.8	5.2
13D14B08	Magnetite	B-1-02	127	32.2		229	58.5	67.7	1114	5.1	59.1	103	2.81	1.08	0.182	1.71		
13D14B10	Magnetite	B-1-04	176	65	6.43	182	60.9	14.3	1234	4.14	44.2	117	1.66	0.48	0.122	2.43	1.97	1
13D14B11	Magnetite	B-1-05	95.9	35.2		187	58	28.9	1274	3.55	24.6	105	1.74	6.41	0.852	6.03		0.96
13D14B12	Magnetite	B-1-06	298	43.1		280	52.1	7.58	1344	6.7	98.7	113	3.28	10.8	3.377	2.64	0.529	1.28
13D14B13	Magnetite	B-1-07	186	60	7.09	247	56.5	8.73	1331	6.04		120	2.29	1.85	0.238	7.27	2.02	
13D14B14	Magnetite	B-1-08	149	26.8		259	47.8	6.58	1328	6.81	17.6	78.3	2.31	1.55	2.913	6.81	0.842	
13D14B16	Magnetite	B-1-09	90.2	12.4		210	49.0	10.3	1320	7.46	31.5	115	0.67	0.85	0.135	1.36		
13D14B17	Magnetite	B-1-10	370	119	2.29	186	48.8	18.4	1307	4.97	24	114	2.04	4.32	2.086	5.66	5.11	
13D14B18	Magnetite	B-1-11	253	30.9		231	52.9	21.7	1311	6.11	42.2	64.7	2.23	2.47	0.873	2.22	2.1	1.04
13D14B19	Magnetite	B-1-12	143	36.3		222	55.4	10.7	1277	5.76	34.1	62.4	2.21	0.52	0.164	0.53		
13D14B22	Magnetite	B-1-15	169	23.3		208	49.2	17.4	1218	6.4		117	2.27	1.36	0.315	0.64		1
13D14B23	Magnetite	B-1-16	60.4	18.3		170	52	30.1	1166	3.74	45.8	89	1.41	0.26	0.206	0.81		1.23
13D14B24	Magnetite	B-1-17	119	27		216	49.2	8.16	1247	6.45	25.2	94.1	2.43	3.71	1.377	4.16	0.925	
13D14B26	Magnetite	B-1-19	111	22.5		261	52.3	15.9	1286	6.11	53.7	99.3	0.89	0.55	0.776	4.54	0.83	
13D14C07	Magnetite	92-O-137-01	43.9	70.8	11.1	4.9	116	39.1	544	20.4	183	1757	4.47	3.13	0.539	28.1	16.4	2.72
13D14C08	Magnetite	92-O-137-02	38.1	46.6	4.07	27.6	118	50.1	337	19.3	157	1431	1.69	2.44		22.8	3.5	
13D14C11	Magnetite	92-O-137-05	41.1	5.5	1.75	30.9	101	54.4	304	16.9	165	1542	2.05	0.15	0.137	1.77		
13D14C12	Magnetite	92-O-137-06	77.7	47.7	7.08	25.4	126	52.1	370	20.4	187	1628	2.92	0.56		1.98		2.26
13D14C13	Magnetite	92-O-137-07	99	86.5	35	41.9	128	33.9	525	26.3	159	1666	2.91	2.32	1.772	41	21.6	1.74
13D14C17	Magnetite	92-O-137-10	72.8	65.1	16.6	20.1	124	21.1	454	17	159	1576	2.53	11.8	2.612	16.3	2.7	1.45
13D14C29	Magnetite	92-O-137-21	32.8	32.3		8.79	119	53.3	372	20.9	190	1710	3	1.12		0.22		
13D14C31	Magnetite	92-O-137-23	96	32.6	5.18	8.31	115		377	20.5	148	1638	3.04	0.82	1.082	0.14		
13D14C33	Magnetite	92-O-137-25	30.2	40.8	14.7	15.3	116	29.2	436	18.1	201	1747	1.23	1.99	1.22	27.2	3.7	1.78
13D14C16	Hematite	92-O-137-09	32.9	14.7	1.68	34.8	117	39.8	317	17.4	183	1457	2.25			0.31		1.32
13D14C20	Hematite	92-O-137-13	18.5	22.2	1.49	21.5	115	39.8	393	17	135	1498	2.86	0.3	1.069	4.74		1.18

13D14C24	Hematite	92-O-137-17	68	16.9	7.12	9.21	128	27.8	364	20.6	157	1551	2.52	1.43	2.438	9.51	4.37	
13D14C26	Hematite	92-O-137-18	59.9	26.3	1.71		117	6.51	284	21	168	1716	3.42	0.54	0.25	2.65		
13D14C27	Hematite	92-O-137-19	68.2	19.2	12.5	6.56	118	12	380	20.9	212	1507	1.84	1.07	0.556	51.8		1.44
13D14C28	Hematite	92-O-137-20	28.4	21.3	1.97	16.3	112	16.2	359	20.4	148	1631	2.27	0.15	0.411	41.7		1.18
13D14C30	Hematite	92-O-137-22	41.5	13.4	4.97		117	4.69	357	17.1	157	1577	1.5	5.17	1.068	0.19	0.637	
13D14C32	Hematite	92-O-137-24	39		2.43	32	103	19.8	390	24.6	152	1748	2.67	0		2.48		1.11
13D14C34	Hematite	92-O-137-26	45	10.2	2.9	13.4	105		370	15.2	177	1722	4.92	0.47	0.492	29.1	0.711	1.25
13D14D07	Magnetite	92-O-99-01	91.3	94.1	9.44	46.3	354	111	930	67.2	199	254	1.15	10.9	9.58	470	11.3	1.84
13D14D08	Magnetite	92-O-99-02	154	126.2	19.6	126	349	145	835	63.8	180	211	0.31	10	24.2	487	13.5	5.44
13D14D09	Magnetite	92-O-99-03	97	75.7	7.32	75	372	167	834	75.4	184	236		8.55	9.66	455	8.06	4.92
13D14D11	Magnetite	92-O-99-05	125	121.7	17.5	60.5	354	92.8	768	71.2	175	207	1.01	23	17.1	436	7.27	3.49
13D14D12	Magnetite	92-O-99-06	74	88.2	4.62	50.4	348	86.9	773	70.1	178	212	0.97	8.56	10	379	8.82	1.64
13D14D13	Magnetite	92-O-99-07	81.6	83.6	11.1	76.5	363	121	1269	73.1	179	186	2.52	17.2	12.9	437	12.3	2.43
13D14D14	Magnetite	92-O-99-08	82.2	76.7	11.7	44.8	367	101	980	72.1	148	227	1.43	12.6	9.93	444	10.1	3.86
13D14D16	Magnetite	92-O-99-09	69.5	95.9	8.48	24.6	375	116	1000	66.4	187	193	1.4	7.16	9.76	303	6.76	1.55
13D14D17	Magnetite	92-O-99-10	143	90	10.7	62.9	350	86.2	975	69	128	229	0.34	7.02	10.7	311	4.59	3.36
13D14D19	Magnetite	92-O-99-12	80.6	79	7.23	8.77	358	105	968	68.5	194	220	1.06	8.42	8.52	318	6.32	3.57
13D14D22	Magnetite	92-O-99-15	80.5	101.5	8.2	43.1	359	87.8	911	68.7	175	208	0.69	8.96	11.1	507	11.5	3.80
13D14D23	Magnetite	92-O-99-16	130	92.6	10.7	66.2	396	94.6	975	75	197	270	1.08	7.59	8.8	428	6.80	4.52
13D14D24	Magnetite	92-O-99-17	119	78.3	6.86	59.2	389	97.6	1033	69.8	174	270	0.64	6.8	5.02	418	7.30	3.24
13D14E08	Magnetite	208-4-1-02	1161	3.1		459	90.2	8.37	7754	27.6		270	1.13	0.31	0.189	5.18		49.3
13D14E09	Magnetite	208-4-1-03	970	5.91		472	87.6	4.89	8146	26.3		268	0.31			8.45		56.4
13D14E10	Magnetite	208-4-1-04	1313	3.49		574	89.9	12.5	8655	25.8		258			0.08	15.8		57.7
13D14E11	Magnetite	208-4-1-05	1647	17.1		692	93.6	13.8	8954	20.1		324	1.15	0.36	0.537	47.2		59.7
13D14E12	Magnetite	208-4-1-06	1703	6.88	5.23	734	94.1	17.7	9335	25.2		346	0.57	0.64	0.296	45.4		49.4
13D14E13	Magnetite	208-4-1-07	1412	20.5		577	92.1	14.1	8316	24.7	21.2	355	0.67	0.29	0.198	31.9	0.51	61
13D14E14	Magnetite	208-4-1-08	1528	16.3		702	98	16.3	9566	21.7	38.4	333	0.86	0.1		11.3	0.503	55.1
13D14E16	Magnetite	208-4-1-09	1350	12.8		462	91.7	6.42	8695	19.1	67.1	282	1.1	5.44	0.101	13.4	0.264	58.6
13D14E17	Magnetite	208-4-1-10	1253	10.6	2.23	571	92	9.77	8416	23.5		277	0.74		0.097	8.01		53.8
13D14E18	Magnetite	208-4-1-11	1427	21.4	2	472	101	12.3	7985	24.9	26.9	335	0.86	0.1	0.391	14.9		48.6
13D14E19	Magnetite	208-4-1-12	1965	9.07	4.13	353	90.3	5.59	8432	20.3		300	0.66	0.15	0.248	12.2		57.8
13D14F07	Magnetite	B-2-01	99.5	12.5		103	322	33.6	2229	11.2	65.3	264	6.01					1.92
13D14F08	Magnetite	B-2-02	105	19.7		106	334	31.4	2227	11	102	228	2.71		0.134	0.89		1.25
13D14F10	Magnetite	B-2-04	73.1	15.7	1.7	67.6	339	50.5	2218	10.2	16.7	208	4.74		0.254	1.33	0.227	
13D14F12	Magnetite	B-2-06	79.8	13.9	2.28	47.5	358	168.7	2258	10.5	118	210	2.92			0.13		
13D14F14	Magnetite	B-2-08	76.4	18.6		62.5	354	70.6	2264	9.7	48.8	191	3.65	0.2	0.942	6.63		1.06
13D14F17	Magnetite	B-2-10	72.9	14	2.39	66	382	34.4	2275	12.7	69.4	205	3.75		1.029	0.13		0.95
13D14F18	Magnetite	B-2-11	77.9	14.6	1.34	75.8	370	117	2301	12.2	25	237	5.45		0.187	1.56		1.24
13D14F19	Magnetite	B-2-12	52.7	13.7		99	373	47.8	2185	12.5	46.8	208	6.4		0.429	1.44		
13D14F22	Magnetite	B-2-15	74.2	7.15	1.41	105	324	144	2227	10.1	118	204	4.61					0.92
13D14F23	Magnetite	B-2-16	81.2	21.1	1.7	99.1	367	99.1	2144	12.3		179	5.01	0.2			0.542	0.95
13D14F26	Magnetite	B-2-18	105	24.1	2.36	65.7	374	16.7	2117	12.8	29.9	228	3.5	0.05				
13D14F29	Magnetite	B-2-21	108	18.3	1.74	85.4	371	25	2132	10.2	31.4	179	5.11			0.06		1.66
13D14F32	Magnetite	B-2-24	69.8	14.4	1.61	73.8	385	116	2144	15.6	111	256	5.69			0.2		1.6
13D14F39	Magnetite	B-2-31	66.1	25.5		76.2	342	183	2256	14.1	87.5	265	3.53			1.2		2.6
13D14F21	Hematite	B-2-14	71	18.2	1.79	156	357	17.4	2048	11	117	221	5.66	0.62	0.179	166	0.964	1.04
13D14F27	Hematite	B-2-19	83	10.1		78.7	429	23.3	2092	12.7	67.3	222	5.36					
13D14F28	Hematite	B-2-20	89.3	16.8		89.8	370	25	2157	10.9	52.8	216	5.96			4		
13D14F30	Hematite	B-2-22	94.9	11.3	1.65	63.3	396	89.5	2144	11.5	89.4	249	6.6			1.26		1.24
13D14F31	Hematite	B-2-23	75.4	10.6		78.9	372	140	2027	10.8	27.5	212	5.39	0.32	0.066	65.7	0.365	
13D14F37	Hematite	B-2-29	123	16.9	2.3	80	354	33	2244	12.6	99.5	272	6.97			8.15		1.93
13D14F38	Hematite	B-2-30	96.3	14.7	2.15	110	349	104	2182	14.1	34.8	342	4.39	0.48	1.503	79.5	0.462	2.94

(continued on next page)

Appendix 1 *(continued)*

Lab no.	Mineral	Sample no.	Ba	Pb	Bi	La	Ce	Pr	Nd	Sm	Eu	Gd	Tb	Dy	Ho	Er	Tm	Yb	Lu
		Detection limit	<0.001	0.037	0.012	0.008	0.012	0.002	<0.001	0.011	0.002	0.010	0.002	0.009	<0.001	0.004	0.003	<0.001	0.002
13D14A07	Magnetite	M-2-01	19.6	2.98	0.748	4.275	24.020	3.251	11.102	1.220	0.144	0.365	0.035	0.057	0.007		0.006	0.134	
13D14A09	Magnetite	M-2-03	2.37	1.66	0.195	0.644	1.889	0.299	1.607		0.030	0.048	0.032			0.046		0.050	
13D14A10	Magnetite	M-2-04	3.07	0.77	0.154	0.197	0.743	0.061	0.733	0.294	0.028			0.075	0.006		0.016	0.024	0.011
13D14A11	Magnetite	M-2-05	3.04	0.56	0.134	0.653	1.569	0.362	0.899	0.258	0.023	0.048			0.006	0.092		0.051	
13D14A12	Magnetite	M-2-06	8.88	7.17	0.996	2.795	10.535	1.743	5.181	0.503	0.149	0.209	0.007	0.028	0.007	0.049	0.006		0.024
13D14A14	Magnetite	M-2-07	4.93	0.92	0.051	1.444	7.498	1.433	5.757	0.792	0.182	0.230	0.074	0.224	0.054	0.087			0.005
13D14A15	Magnetite	M-2-08	21.4	5.45	0.443	1.408	7.729	1.206	3.791	0.517	0.105	0.095	0.013	0.154		0.023	0.011		0.005
13D14A17	Magnetite	M-2-10	6.74	8.33	1.48	1.273	6.139	0.834	2.702	0.398	0.065		0.021	0.166	0.047	0.049	0.006		
13D14A18	Magnetite	M-2-11	1.81	3.13	0.874	0.142	0.829	0.093	0.276	0.052	0.010							0.024	
13D14A20	Magnetite	M-2-13	11.4	6.03	0.439	1.806	10.441	1.546	3.973	1.018	0.101	0.287	0.032	0.110	0.050	0.045	0.017	0.049	0.005
13D14A21	Magnetite	M-2-14	14.8	4.95	0.29	2.334	11.318	1.510	4.899	0.596	0.116	0.048	0.032	0.277	0.013	0.023	0.022	0.025	0.011
13D14A23	Magnetite	M-2-15	17.3	5	0.32	2.543	11.665	1.554	5.542	0.642	0.139	0.122	0.016	0.127	0.005			0.062	0.009
13D14A24	Magnetite	M-2-16	6.32	3.28	0.488	1.559	8.969	1.196	3.786	0.134	0.099	0.275	0.010	0.083	0.036	0.037	0.018	0.020	
13D14A25	Magnetite	M-2-17	25.5	2.16	0.178	3.220	18.963	2.650	7.882	0.881	0.148	0.433	0.052	0.138	0.011	0.041			
13D14A26	Magnetite	M-2-18	8.73	1.71	0.104	1.135	7.841	1.044	2.869	0.315	0.035	0.093		0.050				0.120	0.005
13D14A27	Magnetite	M-2-19	14.1	1.98	0.176	2.138	10.377	1.531	4.736	0.479	0.079	0.141	0.006	0.101	0.012			0.024	
13D14A28	Magnetite	M-2-20	6.25	4.26	1.078	0.690	2.858	0.375	1.364	0.257	0.053	0.091	0.012	0.049			0.021		
13D14A40	Magnetite	M-2-31	15.5	24.8	1.04	3.406	13.467	3.031	10.638	0.920	0.295	0.220	0.022	0.234	0.056	0.282	0.018	0.028	
13D14A41	Magnetite	M-2-32	17.6	15.4	0.358	3.369	15.065	2.248	7.591	0.644	0.259	0.225	0.038	0.368	0.132	0.215	0.013	0.235	0.050
13D14A42	Magnetite	M-2-33	16.7	16.5	0.783	2.763	15.211	2.208	7.979	0.767	0.237	0.257	0.014	0.056	0.047	0.171	0.012		0.006
13D14A44	Magnetite	M-2-35	13.5	11.7	0.213	3.262	18.478	2.402	7.999	1.015	0.260	0.104	0.028	0.282	0.101	0.222	0.029	0.027	
13D14B08	Magnetite	B-1-02	12.3	4.52	0.738	0.390	2.751	0.380	2.634	0.252	0.053	0.176	0.037	0.125	0.012	0.042		0.025	
13D14B10	Magnetite	B-1-04	11.6	5.41	0.817	0.218	0.897	0.144	0.504		0.022		0.021	0.056				0.055	
13D14B11	Magnetite	B-1-05	13.1	2.57	0.104	2.045	12.776	1.986	11.617	1.126	0.256	0.357	0.022	0.204	0.029	0.024	0.045	0.029	
13D14B12	Magnetite	B-1-06	12.5	4.06	0.533	10.591	58.159	8.818	36.011	2.885	0.588	1.306	0.117	0.722	0.078	0.484	0.044	0.335	0.030
13D14B13	Magnetite	B-1-07	16.1	21.6	3.391	2.909	10.934	1.690	5.722	0.133	0.129	0.057	0.064	0.130	0.080	0.109			
13D14B14	Magnetite	B-1-08	5.39	1.38	0.613	2.199	11.219	2.702	9.542	1.619	0.283	0.380	0.160	0.706	0.187	0.441	0.012	0.054	0.024
13D14B16	Magnetite	B-1-09	12.4	3.99	0.576	0.755	0.966	0.624	2.815	0.761	0.057	0.054	0.008	0.092	0.023	0.026			
13D14B17	Magnetite	B-1-10	19.7	3.96	0.615	3.035	20.397	3.431	14.532	1.656	0.333	0.385	0.557	0.439	0.055	0.091		0.072	
13D14B18	Magnetite	B-1-11	12.4	3.37	0.15	5.186	19.879	3.435	12.799	1.293	0.281	0.751	0.044	0.180	0.073	0.174	0.013	0.059	
13D14B19	Magnetite	B-1-12	4.66	2.18	0.241	0.299	1.587	0.393	2.070	0.290	0.017		0.021	0.028	0.014	0.070		0.111	
13D14B22	Magnetite	B-1-15	10.5	1.42	0.14	0.074	0.754	0.071	0.539	0.000	0.031		0.034	0.082	0.020	0.068		0.080	
13D14B23	Magnetite	B-1-16	0.54	2.39	0.32	1.363	3.406	0.529	3.556	0.176	0.027	0.152	0.028	0.029		0.071			0.012
13D14B24	Magnetite	B-1-17	14.4	2.45	0.442	8.825	35.696	5.974	26.353	2.085	0.475	1.082	0.122	0.728	0.049	0.143		0.057	0.006
13D14B26	Magnetite	B-1-19	5.45	0.98	0.115	1.837	10.453	1.644	6.047	1.114	0.135	0.184	0.026	0.156	0.038	0.064	0.006		
13D14C07	Magnetite	92-O-137-01	5.07	43.5	16.6	0.542	4.021	0.409	1.642		0.029		0.068	0.093	0.034	0.042	0.010	0.139	0.020
13D14C08	Magnetite	92-O-137-02	2.93	10.4	4.7	0.251	1.201	0.073	0.329		0.069				0.009				0.016
13D14C11	Magnetite	92-O-137-05		0.72	0.32	0.018	0.198	0.027	0.145		0.012	0.141		0.124			0.009	0.041	
13D14C12	Magnetite	92-O-137-06	0.7	10.6	1.68	0.105	0.850	0.881	0.417	0.318	0.018		0.029	0.118		0.033	0.017		
13D14C13	Magnetite	92-O-137-07	3.74	51.4	13.6	1.166	6.321	0.706	3.766	0.490	0.073	0.164	0.083	0.244	0.106	0.435	0.063	0.144	0.031
13D14C17	Magnetite	92-O-137-10	1.66	17.9	3.48	0.482	4.071	0.982	3.994	0.476	0.216	0.876	0.046	0.715	0.277	0.932	0.021	0.373	0.051
13D14C29	Magnetite	92-O-137-21	3.58	1.07	0.293	0.236	0.328	0.290	0.628		0.015	0.153	0.032		0.022				
13D14C31	Magnetite	92-O-137-23	13.8	1.88	0.468	0.073	0.621	0.120	0.366		0.033			0.084					
13D14C33	Magnetite	92-O-137-25	1.43	13.7	11.7	0.360	2.068	0.200	0.800	0.100	0.109	0.345	0.048	0.712	0.110	0.292	0.011	0.149	0.011
13D14C16	Hematite	92-O-137-09	0.27	0.23	0.262	0.041	0.037		0.245		0.005		0.011						
13D14C20	Hematite	92-O-137-13		1.36	0.288	0.187	0.658	0.207	0.518	0.084	0.054	0.071	0.062	0.092	0.165	0.120	0.037	0.167	
13D14C24	Hematite	92-O-137-17	3.58	9.28	1.594	0.128	0.910	0.219	0.832	0.472	0.118		0.093	1.011	0.151	0.493	0.052	0.237	
13D14C26	Hematite	92-O-137-18	0.29	1.47	0.271	2.046	9.291	0.756	3.007	0.702	0.031		0.062				0.022		
13D14C27	Hematite	92-O-137-19	1.22	4.13	1.051	0.093	0.324	0.111	0.297		0.029		0.010	0.086	0.093	0.058	0.028	0.042	0.009
13D14C28	Hematite	92-O-137-20	2.87	3.13	0.754	0.313	0.794	0.095	0.586	0.083	0.009	0.143	0.010	0.507	0.010	0.589	0.055	0.290	0.018
13D14C30	Hematite	92-O-137-22	2.64	1.32	0.522	0.322	1.337	0.050	0.882		0.030	0.132	0.028	0.078	0.019	0.029		0.038	0.033
13D14C32	Hematite	92-O-137-24		0.84	0.212	0.220	0.309	0.030	0.402		0.010	0.078							
13D14C34	Hematite	92-O-137-26	2.46	4.07	0.58	1.590	4.283	0.565	2.491		0.005	0.225		0.044	0.106	0.149	0.010	0.129	0.009
13D14D07	Magnetite	92-O-99-01	34.7	156	2.80	4.340	12.368	1.987	13.469	4.992	1.477	3.367	0.952	3.930	0.705	1.476	0.207	2.441	0.341
13D14D08	Magnetite	92-O-99-02	102	190	4.80	6.849	10.909	2.892	16.531	5.512	2.309	5.674	1.150	7.993	1.360	3.844	0.383	1.721	0.173

13D14D09	Magnetite	92-O-99-03	24.2	127	3.13	7.411	8.117	3.137	16.460	4.751	1.698	4.256	0.837	4.995	0.648	1.912	0.176	0.748	0.046
13D14D11	Magnetite	92-O-99-05	62.3	147	3.99	4.507	9.893	2.541	17.335	4.378	1.933	6.082	0.982	7.031	1.358	2.774	0.302	1.452	0.087
13D14D12	Magnetite	92-O-99-06	16.6	128	3.13	2.117	6.264	1.000	5.740	3.239	1.177	3.658	0.632	4.379	0.809	1.989	0.174	0.594	0.110
13D14D13	Magnetite	92-O-99-07	74.5	171	2.42	2.645	13.368	1.670	12.759	3.997	1.628	4.020	0.900	6.245	1.010	2.154	0.225	1.099	0.086
13D14D14	Magnetite	92-O-99-08	28	143	3.81	2.297	11.012	1.711	10.183	4.504	1.364	3.603	0.759	5.559	0.766	2.162	0.252	0.999	0.101
13D14D16	Magnetite	92-O-99-09	23.7	121	3.44	2.683	8.499	1.374	7.297	3.624	1.105	3.271	0.527	3.639	0.502	1.622	0.130	0.603	0.092
13D14D17	Magnetite	92-O-99-10	61.8	103	1.98	4.615	10.148	2.156	9.603	2.872	1.295	3.658	0.692	4.556	0.582	1.576	0.110	1.247	0.041
13D14D19	Magnetite	92-O-99-12	24.4	105	2.84	2.454	6.846	1.416	6.901	3.477	1.221	3.207	0.609	4.395	0.643	1.465	0.138	0.695	0.089
13D14D22	Magnetite	92-O-99-15	21.2	142	3.2	6.581	10.176	3.434	17.253	5.721	1.848	4.054	0.822	4.493	0.875	1.452	0.243	1.034	0.106
13D14D23	Magnetite	92-O-99-16	34.1	96.9	5.58	3.504	9.167	1.601	9.183	3.272	1.211	3.162	0.483	4.044	0.693	1.393	0.220	0.776	0.045
13D14D24	Magnetite	92-O-99-17	36.8	107	6.36	4.996	9.929	1.859	9.641	3.300	1.085	2.981	0.447	2.679	0.355	1.273	0.073	0.335	0.044
13D14E08	Magnetite	208-4-1-02	2.79	0.33		0.047	0.096	0.051	0.138	0.155	0.009				0.013		0.006	0.078	
13D14E09	Magnetite	208-4-1-03	0.52	0.35	0.097		0.048		0.103							0.046	0.013	0.029	0.013
13D14E10	Magnetite	208-4-1-04	1.78	0.36	0.029				0.095							0.042	0.012		
13D14E11	Magnetite	208-4-1-05	5.77	3.64	0.075	0.096	0.477	0.156	0.741	0.356	0.078	0.107		0.091	0.007	0.070		0.060	0.007
13D14E12	Magnetite	208-4-1-06	1.58	5.66	0.058	0.030	0.442	0.128	0.811	0.324	0.083	0.118		0.166	0.008	0.050			
13D14E13	Magnetite	208-4-1-07	2.37	3.48	0.068	0.015	0.279	0.064	0.747		0.047	0.118	0.008	0.033	0.008	0.050		0.033	0.007
13D14E14	Magnetite	208-4-1-08	1.93	0.25	0.066		0.026	0.083		0.063	0.005							0.064	0.014
13D14E16	Magnetite	208-4-1-09	1.67	0.18	0.056	0.031	0.054		0.174		0.016				0.016	0.025	0.029	0.099	0.014
13D14E17	Magnetite	208-4-1-10	1.14	0.49			0.026						0.008		0.023				
13D14E18	Magnetite	208-4-1-11	0.77	1.17	0.098	0.045	0.078	0.093	0.281		0.026	0.058		0.096		0.191		0.063	
13D14E19	Magnetite	208-4-1-12	3.69	0.64			0.252	0.063	0.458	0.064	0.025	0.117	0.024			0.049	0.014		
13D14F07	Magnetite	B-2-01			0.033	0.058	0.139	0.010	0.108		0.012				0.015				
13D14F08	Magnetite	B-2-02		0.36	0.031	0.014	0.060			0.060		0.054	0.022	0.030	0.014		0.019		
13D14F10	Magnetite	B-2-04	0.17	0.21	0.02				0.049	0.227	0.038	0.103	0.021	0.144	0.034	0.022			
13D14F12	Magnetite	B-2-06	0.17	0.19	0.04						0.011		0.014						
13D14F14	Magnetite	B-2-08	20.4	1.01	0.04	0.066	0.134	0.009	0.049		0.033	0.102	0.028	0.346	0.034	0.162	0.031	0.136	0.018
13D14F17	Magnetite	B-2-10	0.48	0.46	0.028		0.213	0.170	0.183	0.106	0.016		0.013		0.097	0.089	0.040	0.102	0.034
13D14F18	Magnetite	B-2-11	2.48	1	0.044	0.073	0.300	0.020	0.325		0.090		0.015	0.128	0.031	0.026		0.211	
13D14F19	Magnetite	B-2-12		0.22	0.021	2.296	4.826	0.464	2.645	0.419	0.081	0.162	0.022	0.336	0.037	0.228	0.032	0.029	0.006
13D14F22	Magnetite	B-2-15		0.09	0.031						0.006							0.029	0.084
13D14F23	Magnetite	B-2-16	13.5	0.51	0.046		0.067	0.010			0.004								
13D14F26	Magnetite	B-2-18	0.74	0.23	0.084														
13D14F29	Magnetite	B-2-21		0.42	0.012	0.015							0.016			0.028		0.064	
13D14F32	Magnetite	B-2-24	0.25	0.47		0.076	0.232	0.013	0.144		0.004								
13D14F39	Magnetite	B-2-31	1.42	0.23		0.044	0.136				0.005		0.036						
13D14F21	Hematite	B-2-14	2.36	11.5	0.223	0.527	1.970	0.245	1.495	0.239	0.072	0.053	0.029	0.121	0.051			0.143	
13D14F27	Hematite	B-2-19		0.28	0.123				0.112		0.005	0.113					0.041		
13D14F28	Hematite	B-2-20		0.69	0.093	0.035	0.046	0.024	0.200		0.008				0.009		0.016		
13D14F30	Hematite	B-2-22	0.19	0.98	0.122	0.074	0.150	0.020										0.030	
13D14F31	Hematite	B-2-23	0.79	2.2	0.03	0.040	0.555	0.194	0.228	0.349	0.007			0.175					
13D14F37	Hematite	B-2-29		2.11	0.237		0.229	0.026	0.071		0.020							0.039	
13D14F38	Hematite	B-2-30	4.2	9.59	0.134	0.626	1.647	0.436	1.440	0.651	0.148	0.582	0.175	0.494	0.106	0.125	0.035	0.158	0.012

References

Bai, G., 2012. The research history and our understanding of the Bayan Obo Fe-REE-Nb deposit. Acta Geol. Sin. 86, 679–682 (in Chinese).

Bai, G., Yuan, Z.X., Wu, C.Y., Zhang, Z.Q., Zheng, L., 1996. Demonstration on the Geological Features and Genesis of the Bayan Obo Ore Deposit. Geological Publishing House, Beijing (in Chinese with English abstract).

Baker, T., Van Achterberg, E., Ryan, C.G., Lang, J.R., 2004. Composition and evolution of ore fluids in a magmatic-hydrothermal skarn deposit. Geology 32, 117–120.

Beaudoin, G., Dupuis, C., 2009. Iron-oxide trace element fingerprinting of mineral deposit types. In: Corriveau, L., Mumin, A.H. (Eds.), Exploring for Iron Oxide Copper-Gold Deposits: Canada and Global Analogues: GAC Short Course Notes, pp. 107–121.

Campbell, L.S., Henderson, P., 1997. Apatite paragenesis in the Bayan Obo REE-Nb-Fe ore deposit, Inner Mongolia, China. Lithos 42, 89–103.

Campbell, L.S., Compston, W., Sircombe, K.N., Wilkinson, C.C., 2014. Zircon from the east orebody of the Bayan Obo Fe-Nb-REE deposit, China, and SHRIMP ages for carbonatite-related magmatism and REE mineralization events. Contrib. Mineral. Petrol. 168, 1041–1063.

Cao, R., Zhu, S., Wang, J., 1994. Source materials for the Bayan Obo Fe-REE ore deposit and problems on the genetic theory. Sci. China Ser. B 24, 1298–1307 (in Chinese with English abstract).

Carew, M.J., 2004. Controls on Cu-Au Mineralisation and Fe Oxide Metasomatism in the Eastern Fold Belt, NW Queensland, Australia(Ph.D. thesis) James Cook University, Queensland.

Chao, E., Back, J., Minkin, J., Yinchen, R., 1992. Host-rock controlled epigenetic, hydrothermal metasomatic origin of the Bayan Obo REE-Fe-Nb ore deposit, Inner Mongolia, PRC. Appl. Geochem. 7, 443–458.

Chao, E.C.T., Tatsumoto, M., McKee, E.H., 1995. Caledonian subduction, repeated activation, and multiple episodes of mineralization of the Bayan Obo REE-Fe-Nb ore deposit, Inner Mongolia, China. Glob. Tecton. Metallogeny 5, 37–39.

Chao, E.C.T., Back, J.M., Minkin, J.A., Tatsumoto, M., Wang, J., Conrad, J.E., McKee, E.H., Hou, H., Meng, Q., Huang, S., 1997. The sedimentary carbonate-hosted giant Bayan Obo REE-Fe-Nb ore deposit of Inner Mongolia, China: a cornerstone example for giant polymetallic ore deposits of hydrothermal origin. US Geol. Surv. Bull. 2143, 5.

Chen, W.T., Zhou, M.-F., Li, X., Gao, J.-F., Hou, K., 2015. In-situ LA-ICP-MS trace elemental analyses of magnetite: the Khetri copper belt in Rajasthan province, NW India. Ore Geol. Rev. 65, 929–939 (in this issue).

Chung, D., Zhou, M.-F., Gao, J.-F., Chen, W.T., 2015. In-situ LA-ICP-MS trace elemental analyses of magnetite: the late Palaeoproterozoic Sokoman Iron Formation in the Labrador Trough, Canada. Ore Geol. Rev. 65, 917–928 (in this issue).

Dare, S.A.S., Barnes, S.J., Beaudoin, G., 2012. Variation in trace element content of magnetite crystallized from a fractionating sulfide liquid, Sudbury, Canada: implications for provenance discrimination. Geochim. Cosmochim. Acta 88, 27–50.

Drew, L.J., Qingrun, M., Weijun, S., 1990. The Bayan Obo iron-rare-earth-niobium deposits, Inner Mongolia, China. Lithos 26, 43–65.

Dupuis, C., Beaudoin, G., 2011. Discriminant diagrams for iron oxide trace element fingerprinting of mineral deposit types. Mineral. Deposita 46, 1–17.

Einaudi, M.T., Meinert, L.D., Newberry, R.J., 1981. Skarn deposits. Econ. Geol. 75, 317–391.

Fan, H.R., Hu, F.F., Yang, K.F., Wang, K.Y., Liu, Y.S., 2009. Geochronology framework of late Paleozoic dioritic-granitic plutons in the Bayan Obo area, Inner Mongolia, and tectonic significance. Acta Petrol. Sin. 25, 2933–2938 (in Chinese with English abstract).

Fan, H.R., Yang, K.F., Hu, F.F., Wang, K.Y., Zhai, M.G., 2010. Zircon geochronology of basement rocks from the Bayan Obo area, Inner Mongolia, and tectonic implications. Acta Petrol. Sin. 26, 1342–1350 (in Chinese with English abstract).

Fan, H.-R., Hu, F.-F., Yang, K.-F., Pirajno, F., Liu, X., Wang, K.-Y., 2014. Integrated U-Pb and Sm-Nd geochronology for a REE-rich carbonatite dyke at the giant Bayan Obo REE deposit, Northern China. Ore Geol. Rev. 63, 510–519.

Fang, T., Qiu, Y., 1997. Stable isotopic composition characteristics of REE minerals from the Bayan Obo ore deposit and their genetic implications. Miner. Depos. 16, 31–40 (in Chinese with English abstract).

Fang, T., Qiu, Y.Z., Chen, C.Y., Chen, H.X., Wang, Y.J., 1995. Oxygen isotopic aspects of apatite in Bayan Obo ore deposit. Acta Miner. Sin. 15, 163–167 (in Chinese with English abstract).

Gao, J.F., Zhou, M.F., LightFoot, P.C., Wang, C.Y., Qi, L., Sun, M., 2013. Sulfide saturation and magma emplacement in the formation of the Permian Huangshandong Ni-Cu sulfide deposit, Xinjiang, Northwestern China. Econ. Geol. 108, 1833–1848.

Hou, Z., 1989. The Bayan Obo Fe-Nb-REE-deposit: its basic geological features, metallogenesis and genetic model. Geol. Prospect. 25, 1–5 (in Chinese with English abstract).

Hu, H., Li, J.-W., Lentz, D., Ren, Z., Zhao, X.-F., Deng, X.-D., Hall, D., 2013. Dissolution–reprecipitation process of magnetite from the Chengchao iron deposit: insights into ore genesis and implication for *in-situ* chemical analysis of magnetite. Ore Geol. Rev. 57, 393–405.

Huang, X.W., Zhou, M.F., Qi, L., Gao, J.F., Wang, Y.W., 2013. Re-Os isotopic ages of pyrite and chemical composition of magnetite from the Cihai magmatic-hydrothermal Fe deposit, NW China. Miner. Deposita 48, 925–946.

Huang, X.W., Qi, L., Meng, Y.M., 2014. Trace element geochemistry of magnetite from the Fe(-Cu) deposits in the Hami region, Eastern Tianshan Orogenic Belt, NW China. Acta Geol. Sin. 88, 176–195.

Huang, X.W., Gao, J.F., Qi, L., Zhou, M.F., 2015. In-situ LA-ICP-MS trace elemental analyses of magnetite and Re-Os dating of pyrite: the Tianhu hydrothermally remobilized sedimentary Fe deposit, NW China. Ore Geol. Rev. 65, 900–916 (in this issue).

IGCAS (Institute of Geochemistry, Chinese Academy of Sciences), 1988. The Geochemistry of the Bayan Obo Ore Deposit (in Chinese with English Abstract). Science Press, Beijing.

Ilton, E.S., Eugster, H.P., 1989. Base metal exchange between magnetite and a chloride-rich hydrothermal fluid. Geochim. Cosmochim. Acta 53, 291–301.

Kynicky, J., Smith, M.P., Xu, C., 2012. Diversity of rare earth deposits: the key example of China. Elements 8, 361–367.

Le Bas, M.J., Kellere, J., Tao, K., Wall, F., William, C.T., Zhang, P., 1992. Carbonatite dykes at Bayan Obo, Inner Mongolia, China. Mineral. Petrol. 46, 195–228.

Le Bas, M.J., Spiro, B., Yang, X., 1997. Oxygen, carbon and strontium isotope study of the carbonatitic dolomite host of the Bayan Obo Fe-Nb-*REE* deposit, Inner Mongolia, N China. Mineral. Mag. 61, 531–541.

Ling, M.-X., Liu, Y.-L., Williams, I.S., Teng, F.-Z., Yang, X.-Y., Ding, X., Wei, G.-J., Xie, L.-H., Deng, W.-F., Sun, W.-D., 2013. Formation of the world's largest REE deposit through protracted fluxing of carbonatite by subduction-derived fluids. Sci. Rep. 3, 1–8.

Ling, M.-X., Zhang, H., Li, H., Liu, Y.-L., Liu, J., Li, L.-Q., Li, C.-Y., Yang, X.-Y., Sun, W., 2014. The Permian-Triassic granitoids in Bayan Obo, North China Craton: a geochemical and geochronological study. Lithos 190–191, 430–439.

Liu, P.P., Zhou, M.-F., Chen, W.T., Gao, J.-F., Huang, X.-W., 2015. In-situ LA-ICP-MS trace elementa analyses of magnetite: Fe–Ti–(V) oxide-bearing mafic–ultramafic layered intrusions of the Emeishan Large Igneous Province, SW China. Ore Geol. Rev. 65, 853–871 (in this issue).

Meinert, L.D., 1992. Skarns and skarn deposits. Geosci. Can. 19, 145–162.

Meng, Q., 1982. The genesis of the host rock-dolomite of the Bayan Obo iron ore deposits and the analysis of its sedimentary environment. Geol. Rev. 28, 481–489 (in Chinese with English abstract).

Meng, Q., Drew, L.J., 1992. Study on oxygen and carbon isotope and the implication for genesis of Baiyan Obo ore-bearing H_8 dolomite. Contrib. Geol. Miner. Resour. Res. 7, 46–54 (in Chinese with English abstract).

Müller, B., Axelsson, M.D., Öhlander, B., 2003. Trace elements in magnetite from Kiruna, northern Sweden, as determined by LA-ICP-MS. GFF 125, 1–5.

Nadoll, P., Mauk, J.L., Hayes, T.S., Koenig, A.E., Box, S.E., 2012. Geochemistry of magnetite from hydrothermal ore deposits and host rocks of the Mesoproterozoic Belt Supergroup, United States. Econ. Geol. 107, 1275–1292.

Nadoll, P., Angerer, T., Mauk, J.L., French, D., Walshe, J., 2014. The chemistry of hydrothermal magnetite: a review. Ore Geol. Rev. 61, 1–32.

Qiu, Y.Z., Wen, H.J., Zhang, Q., 2003. Rb-Sr isochron age of gabbros from the Bayan Obo deposit. Ninth Annual Conference Symposium of Chinese Society for Mineralogy. Petrology and Geochemistry, p. 35 (in Chinese).

Qiu, Y.Z., Qin, C.J., Zhou, G.F., Wen, H.J., Liu, S.R., Gong, G.H., Wang, Z.G., Zhang, T.R., Xiao, G.W., 2008. New chronology data of Bayan Obo deposit. In: Chen, Y.C. (Ed.), Ninth National Conference of Mineral Deposit. Geological Publishing House, Beijing, pp. 477–479 (in Chinese).

Qiu, Y.Z., Wen, H.J., Qin, C.J., 2011. Precise determination of the age of Hercynian granitoids and discovery of Yanshanian granitoids. Acta Miner. Sin. 31, 631–632 (in Chinese).

Rudnick, R.L., Gao, S., 2003. Composition of the continental crust. In: Holland, H.D., Turekian, K.K. (Eds.), Treatise on geochemistry. Elsevier-Pergaman, Oxford, pp. 1–64.

Rusk, B.G., Oliver, N., Brown, A., Lilly, R., Jungmann, D., 2009. Barren magnetite breccias in the Cloncurry region, Australia; comparisons to IOCG deposits. Smart science for exploration and mining. Proceedings of the 10th Biennial Society for Geology Applied to Mineral Deposits (SGA) Meeting. Townsville, pp. 656–658.

Singoyi, B., Danyushevsky, L., Davidson, G.J., Large, R., Zaw, K., 2006. Determination of trace elements in magnetites from hydrothermal deposits using the LA ICP-MS technique. SEG Keystone Conference. CD-ROM, Denver, USA.

Smith, M., Wu, C., 2013. The geology and genesis of the Bayan Obo Fe-REE-Nb deposit: a review. In: Porter, T.M. (Ed.), Hydrothermal Iron Oxide Copper-Gold and Related Deposits: A Global Perspective. PGE Publishing, Adelaide, pp. 271–281.

Smith, M., Henderson, P., Campbell, L., 2000. Fractionation of the REE during hydrothermal processes: constraints from the Bayan Obo Fe-REE-Nb deposit, Inner Mongolia, China. Geochim. Cosmochim. Acta 64, 3141–3160.

Smith, M.P., Campbell, L.S., Kynicky, J., 2015. A review of the genesis of the world class Bayan Obo Fe-REE-Nb deposits, Inner Mongolia, China: Multistage processes and outstanding questions. Ore Geol. Rev. 64, 459–476.

Sun, J., Zhu, X., Chen, Y., Fang, N., 2013. Iron isotopic constraints on the genesis of Bayan Obo ore deposit, Inner Mongolia, China. Precambrian Res. 235, 88–106.

Tao, K., Yang, Z., Zhang, P., Wang, W., 1998. Systematic geological investigation on carbonatite dykes in Bayan Obo, Inner mongolia, China. Sci. Geol. Sin. 33, 73–83 (in Chinese with English abstract).

Taylor, S.R., McLennan, S.M., 1985. The Continental Crust: Its Composition and Evolution. Blackwell Scientific Publisher, Palo Alto, CA, pp. 57–72.

Tu, G., 1998. The unique nature in ore composition, geological background and metallogenic mechanism of non-conventional superlarge ore deposits: a preliminary discussion. Sci. China Ser. D Earth Sci. 41, 1–6.

Wang, K., Fan, H., Yang, K., Hu, F., Ma, Y., 2010. Bayan Obo carbonatites: texture evidence from polyphase intrusive and extrusive carbonatites. Acta Geol. Sin. 84, 1365–1376.

Wei, J., Shangguan, Z., 1983. Oxygen isotope composition of magnetite and hematite in Baiyun Ebo iron deposit, Inner Mongolia. Sci. Geol. Sin. 217–224 (in Chinese with English abstract).

Wu, C., 2008. Bayan Obo controversy: carbonatites versus Iron Oxide-Cu-Au-(REE-U). Resour. Geol. 58, 348–354.

Xiao, R., Shi, S., An, G., Zhang, H., Fei, H., 2003. Genetic characteristic of hydrothermal sedimentation of k-rich slate in Baiyun'ebo mine, Inner Mongolia. Geoscience 17, 281–286 (in Chinese with English abstract).

Yang, Z., Drew, L.J., 1994. On the hot-water sedimentary origin of dolomite-host rock of Bayan Obo deposits, Inner Mongolia, China. Contrib. Geol. Miner. Resour. Res. 9, 39–48 (in Chinese with English abstract).

Yang, X.-Y., Sun, W.-D., Zhang, Y.-X., Zheng, Y.-F., 2009. Geochemical constraints on the genesis of the Bayan Obo Fe–Nb–REE deposit in Inner Mongolia, China. Geochim. Cosmochim. Acta 73, 1417–1435.

Yang, K.-F., Fan, H.-R., Santosh, M., Hu, F.-F., Wang, K.-Y., 2011. Mesoproterozoic carbonatitic magmatism in the Bayan Obo deposit, Inner Mongolia, North China: constraints for the mechanism of super accumulation of rare earth elements. Ore Geol. Rev. 40, 122–131.

Zeng, J., Wang, M., Qu, W., 1981. The genesis of magnetite from the Bayan Obo Fe deposit. J. Mineral. Petrol. 44–58 (in Chinese).

Zhang, P.S., Yang, Z.M., Tao, K.J., Yang, X.M., 1995. Mineralogy and geology of rare earth elements in China. Science Press, Beijing (in Chinese with English abstract).

Zhang, Z.Q., Yuan, Z.X., Tang, S.H., Bai, G., Wang, J.H., 2003. Age and geochemistry of the Bayan Obo ore deposit. Geological Publishing House, Beijing (in Chinese with English abstract).

Zhang, D., Rusk, B., Oliver, N., Dai, T., 2011. Trace element geochemistry of magnetite from the Ernest Henry IOCG Deposit, Australia. 11th biennial meeting SGA 2011-Let's talk ore deposits. Antofagasta, Chile.

Zhao, W.W., Zhou, M.-F., 2015. In-situ LA–ICP-MS trace elemental analyses of magnetite: The Mesozoic Tengtie skarn Fe deposit in the Nanling Range, South China. Ore Geol. Rev. 65, 872–883 (in this issue).